Semiclassical theory for spatial density oscillations in fermionic systems

J. Roccia, M. Brack, and A. Koch

Institute for Theoretical Physics, University of Regensburg, D-93040 Regensburg, Germany

We investigate the particle and kinetic-energy densities for a system of N fermions bound in a local (mean-field) potential $V(\mathbf{r})$. We generalize a recently developed semiclassical theory [J. Roccia and M. Brack, Phys. Rev. Lett. **100**, 200408 (2008)] in which the densities are calculated in terms of the closed orbits of the corresponding classical system to $D > 1$ dimensions. We regularize the semiclassical results (i) for the $U(1)$ symmetry breaking occurring for spherical systems at $r=0$ and (ii) near the classical turning points where the Friedel oscillations are predominant and well reproduced by the shortest orbit going from r to the closest turning point and back. For systems with spherical symmetry, we show that there exist two types of oscillations which can be attributed to radial and nonradial orbits, respectively. The semiclassical theory is tested against exact quantum-mechanical calculations for a variety of model potentials. We find a very good overall numerical agreement between semiclassical and exact numerical densities even for moderate particle numbers N. Using a "local virial theorem," shown to be valid (except for a small region around the classical turning points) for arbitrary local potentials, we can prove that the Thomas-Fermi functional $\tau_{\mathrm{TF}}[\rho]$ reproduces the oscillations in the quantum-mechanical densities to first order in the oscillating parts.

PACS number(s): 05.30.Fk, 03.65.Sq, 03.75.Ss, 71.10.−w

I. INTRODUCTION

Recent experimental success confining fermion gases in magnetic traps [1] has led to renewed interest in theoretical studies of confined degenerate fermion systems at zero [2–11] and finite temperatures [12,13]. According to the density-functional theory (DFT) [14–16], the local particle density $\rho(\mathbf{r})$ is the key ingredient of a system of interacting fermions in that it contains all information about its ground state. In this paper, we study the oscillations in the particle density $\rho(\mathbf{r})$ and in different forms of the kinetic-energy density of N fermions bound in a local potential $V(\mathbf{r})$. Although we treat the particles as noninteracting, we keep in mind that this potential models the self-consistent Kohn-Sham (KS) potential obtained for an *interacting system in the mean-field approximation*. We shall also consider potentials with infinitely steep walls, so-called "billiards," which have been shown to be good approximations to the self-consistent mean fields of quantum dots [17] or metal clusters [18] with many particles.

A semiclassical theory for spatial density oscillations has been developed recently in [19]. Using Gutzwiller's semiclassical Green's function [20], expressions for the oscillating parts of spatial densities of fermionic systems were given in terms of the *closed orbits* of the corresponding classical system. The semiclassical theory was shown in [19] to reproduce very accurately the quantum oscillations in the spatial densities of one-dimensional systems, even for moderate particle numbers N, and some general results have also been given for arbitrary higher-dimensional spherical potentials $V(r)$.

In this paper, we present in more detail the semiclassical closed-orbit theory developed in [19] and apply it explicitly for a variety of potentials in $D > 1$ dimensions. We find overall a good agreement between the quantum-mechanical and the semiclassical densities.

The paper is organized as follows. In Sec. II, we give the basic definitions of the quantum-mechanical spatial densities. In Sec. II B, we discuss the asymptotic (extended) Thomas-

Fermi (TF) limits for $N \rightarrow \infty$ and emphasize the existence of two types of density oscillations occurring in potentials for $D > 1$ with spherical symmetry (except for isotropic harmonic oscillators).

Section III is devoted to the semiclassical closed-orbit theory for spatial density oscillations. In Secs. III A–III D, we review the basic equations and former results, including also details that were not presented in [19]. In Secs. III E and III F, we extend the semiclassical theory to higher-dimensional systems ($D > 1$) and test its results for various model potentials against exact quantum-mechanical densities. In Sect. III E 3, we discuss the regularization necessary in spherical systems for $D > 1$ near the center ($r=0$), where a $U(1)$ symmetry breaking occurs for $r > 0$. In a separate publication [21], we have presented the analytical determination and classification of all closed orbits in the two-dimensional circular billiard and give analytical results of the semiclassical theory for the spatial density oscillations in this system. Some of the numerical results for the densities are included in Sec. III E 4 of the present paper.

In Sec. IV, we present regularizations of the spatial densities near the classical turning points, where the semiclassical theory diverges, both for smooth potentials and for billiard systems. Section V contains some general results valid for finite fermion systems such as trapped fermionic gases or metallic clusters. We discuss there, in particular, a "local virial theorem" and, as its direct consequence, the extended validity of the TF functional $\tau_{\mathrm{TF}}[\rho]$.

Throughout this paper, we only treat the zero-temperature ground state of an N-particle system. In the Appendix, we outline how to include finite temperatures for grand-canonical ensembles in the semiclassical theory.

II. QUANTUM-MECHANICAL DENSITIES

A. Basic definitions and ingredients

Let us recall some basic quantum-mechanical definitions using the same notation as in [10]. We start from the station-

ary Schrödinger equation for particles with mass m, bound by a local potential $V(\mathbf{r})$ with a discrete energy spectrum $\{E_n\}$,

$$\left\{-\frac{\hbar^2}{2m}\nabla^2 + V(\mathbf{r})\right\}\phi_n(\mathbf{r}) = E_n\phi_n(\mathbf{r}). \qquad (1)$$

We order the spectrum and choose the energy scale such that $0 < E_1 \leq E_2 \leq \ldots \leq E_n \leq \ldots$. We consider a system with an even number N of fermions with spin $s = 1/2$ filling the lowest levels and define the particle density by

$$\rho(\mathbf{r}) := 2\sum_{E_n \leq \lambda}|\phi_n(\mathbf{r})|^2, \quad \int \rho(\mathbf{r})d^D r = N. \qquad (2)$$

Hereby, λ is the Fermi energy and the factor 2 accounts for the fact that due to spin and time-reversal symmetry, each state n is at least twofold degenerate. Further degeneracies, which may arise for $D > 1$, will not be spelled out but included in the summations over n. For the kinetic-energy density, we consider two different definitions [22]:

$$\tau(\mathbf{r}) := -\frac{\hbar^2}{2m}2\sum_{E_n \leq \lambda}\phi_n^*(\mathbf{r})\nabla^2\phi_n(\mathbf{r}), \qquad (3)$$

$$\tau_1(\mathbf{r}) := \frac{\hbar^2}{2m}2\sum_{E_n \leq \lambda}|\nabla\phi_n(\mathbf{r})|^2, \qquad (4)$$

which upon integration both yield the exact total kinetic energy. Due to the assumed time-reversal symmetry, the two above functions are related by

$$\tau(\mathbf{r}) = \tau_1(\mathbf{r}) - \frac{1}{2}\frac{\hbar^2}{2m}\nabla^2\rho(\mathbf{r}). \qquad (5)$$

An interesting, and for the following discussion, convenient quantity is their average

$$\xi(\mathbf{r}) := \frac{1}{2}[\tau(\mathbf{r}) + \tau_1(\mathbf{r})]. \qquad (6)$$

For harmonic oscillators, it has been observed [4,10,23] that inside the system (i.e., sufficiently far from the surface region), $\xi(\mathbf{r})$ is a smooth function of the coordinates, whereas $\tau(\mathbf{r})$ and $\tau_1(\mathbf{r})$, like the density $\rho(\mathbf{r})$, exhibit characteristic shell oscillations that are opposite in phase for τ and τ_1. We can express $\tau(\mathbf{r})$ and $\tau_1(\mathbf{r})$ in terms of $\xi(\mathbf{r})$ and $\nabla^2\rho(\mathbf{r})$,

$$\tau(\mathbf{r}) = \xi(\mathbf{r}) - \frac{1}{4}\frac{\hbar^2}{2m}\nabla^2\rho(\mathbf{r}), \qquad (7)$$

$$\tau_1(\mathbf{r}) = \xi(\mathbf{r}) + \frac{1}{4}\frac{\hbar^2}{2m}\nabla^2\rho(\mathbf{r}), \qquad (8)$$

so that $\rho(\mathbf{r})$ and $\xi(\mathbf{r})$ can be considered as the basic densities characterizing our systems. Equations (2)–(8) are exact for arbitrary potentials $V(\mathbf{r})$. For any even number N of particles, they can be computed once the quantum-mechanical wave functions $\phi_n(\mathbf{r})$ are known. As mentioned in Sec. I, the potential $V(\mathbf{r})$ can be considered to represent the self-consistent mean field of an interacting system of fermions obtained in

the DFT approach. The single-particle wave functions $\phi_n(\mathbf{r})$ are then the Kohn-Sham orbitals [15] and $\rho(\mathbf{r})$ is (ideally) the ground-state particle density of the interacting system.

For later reference, we express the densities (2)–(4) in terms of the Green's function in the energy representation, which in the basis $\{\phi_n(\mathbf{r})\}$ is given by

$$G(E,\mathbf{r},\mathbf{r}') = \sum_n \frac{\phi_n^\star(\mathbf{r})\phi_n(\mathbf{r}')}{E + i\epsilon - E_n}, \quad (\epsilon > 0). \qquad (9)$$

Using the identity $1/(E+i\epsilon-E_n) = \mathcal{P}[1/(E-E_n)] - i\pi\delta(E-E_n)$, where $\mathcal{P}$ is the Cauchy principal value, one can write the densities as

$$\rho(\mathbf{r}) = -\frac{1}{\pi}\text{Im}\int_0^\lambda dE\, G(E,\mathbf{r},\mathbf{r}')|_{\mathbf{r}'=\mathbf{r}}, \qquad (10)$$

$$\tau(\mathbf{r}) = \frac{\hbar^2}{2\pi m}\text{Im}\int_0^\lambda dE\, \nabla_{\mathbf{r}'}^2 G(E,\mathbf{r},\mathbf{r}')|_{\mathbf{r}'=\mathbf{r}}, \qquad (11)$$

$$\tau_1(\mathbf{r}) = -\frac{\hbar^2}{2\pi m}\text{Im}\int_0^\lambda dE\, \nabla_{\mathbf{r}}\nabla_{\mathbf{r}'}G(E,\mathbf{r},\mathbf{r}')|_{\mathbf{r}'=\mathbf{r}}, \qquad (12)$$

whereby the subscript of the nabla operator ∇ denotes the variable on which it acts.

The density of states $g(E)$ of the system (1) is given by a sum of Dirac delta functions, which can be expressed as a trace integral of the Green's function

$$g(E) = \sum_n \delta(E - E_n) = -\frac{1}{\pi}\text{Im}\int d^D r\, G(E,\mathbf{r},\mathbf{r}')|_{\mathbf{r}'=\mathbf{r}}. \qquad (13)$$

The particle number can then also be obtained as

$$N = N(\lambda) = 2\int_0^\lambda dE\, g(E). \qquad (14)$$

Due to the discreteness of the spectrum, $N(\lambda)$ is a monotonously increasing staircase function and consequently the function $\lambda(N)$, too, is a monotonously increasing staircase function.

B. Asymptotic quantum-mechanical results

1. Thomas-Fermi limits and oscillating parts

In the limit $N \to \infty$, the densities are expected to go over into the approximations obtained in the TF theory [24]. These are given, for any local potential $V(\mathbf{r})$, by

$$\rho_{\text{TF}}(\mathbf{r}) = \frac{4}{D}\frac{1}{\Gamma(D/2)}\left(\frac{m}{2\pi\hbar^2}\right)^{D/2}[\lambda_{\text{TF}} - V(\mathbf{r})]^{D/2}, \qquad (15)$$

$$(\tau_1)_{\text{TF}}(\mathbf{r}) = \xi_{\text{TF}}(\mathbf{r}) = \tau_{\text{TF}}(\mathbf{r}), \qquad (16)$$

$$\tau_{\text{TF}}(\mathbf{r}) = \frac{4}{(D+2)}\frac{1}{\Gamma(D/2)}\left(\frac{m}{2\pi\hbar^2}\right)^{D/2}[\lambda_{\text{TF}} - V(\mathbf{r})]^{D/2+1}. \qquad (17)$$

These densities are defined only in the classically allowed regions where $\lambda_{\text{TF}} \geq V(\mathbf{r})$ and the Fermi energy λ_{TF} is de-

fined such as to yield the correct particle number N upon integration of $\rho_{TF}(\mathbf{r})$ over all space. The direct proof that the quantum-mechanical densities, as defined in Sec. II in terms of the wave functions of a smooth potential, reach the above TF limits for $N \to \infty$ is by no means trivial. It has been given for isotropic harmonic oscillators in arbitrary dimensions in Ref. [10].

The TF densities (15)–(17) fulfill the following functional relation:

$$\tau_{TF}(\mathbf{r}) = \tau_{TF}[\rho_{TF}(\mathbf{r})] = \frac{\hbar^2}{2m} \frac{4\pi D}{(D+2)} \left[\frac{D}{4} \Gamma\left(\frac{D}{2}\right) \right]^{2/D} \rho_{TF}^{1+2/D}(\mathbf{r}),$$
(18)

which will be investigated further below.

For smooth potentials in $D > 1$ dimensions, next-to-leading order terms in $1/N$ modify the smooth parts of the spatial densities, which are obtained in the extended Thomas-Fermi (ETF) model as corrections of higher order in $\hbar$ through an expansion in terms of gradients of the potential [25]. These corrections usually diverge at the classical turning points and can only be used sufficiently far from the turning points, i.e., in the interior of the system. We do not reproduce the ETF densities here but refer to [26] (chapter 4) where they are given for arbitrary smooth potentials in $D = 2$ and 3 dimensions and to [10] where explicit results are given for spherical harmonic oscillators in $D = 2$ and 4 dimensions.

This leads us to decompose the densities in the following way:

$$\rho(\mathbf{r}) = \rho_{(E)TF}(\mathbf{r}) + \delta\rho(\mathbf{r}),$$
(19)

$$\tau(\mathbf{r}) = \tau_{(E)TF}(\mathbf{r}) + \delta\tau(\mathbf{r}),$$
(20)

$$\tau_1(\mathbf{r}) = (\tau_1)_{(E)TF}(\mathbf{r}) + \delta\tau_1(\mathbf{r}),$$
(21)

$$\xi(\mathbf{r}) = \xi_{(E)TF}(\mathbf{r}) + \delta\xi(\mathbf{r}).$$
(22)

For $D = 1$ and for billiard systems [27], the subscripts TF and the explicit relations (15)–(17) hold. The oscillating parts $\delta\rho(\mathbf{r})$, etc. are the main objects of this paper.

2. Two types of oscillating parts in spherical systems

We have investigated the density oscillations in various potentials in $D > 1$ dimensions with *radial symmetry* such that $V(\mathbf{r}) = V(r)$, where $r = |\mathbf{r}|$. We found that, generally, there exist two types of oscillations in their spatial densities:

(i) regular, short-ranged oscillations with a constant wavelength in the radial variable r over the whole region, and

(ii) irregular, long-ranged oscillations whose wavelength decreases with increasing r.

An example is shown in Fig. 1 for a spherical billiard with unit radius containing $N = 100\ 068$ particles. Note the irregular, long-ranged oscillations of $\xi(r)$ around its bulk value [27] ξ_{TF} seen in the upper panel. In the lower panel, where we exhibit only an enlarged region around the bulk value, we see that $\tau(r)$ and $\tau_1(r)$ oscillate regularly around $\xi(r)$, but much faster than $\xi(r)$ itself and with opposite phases. The
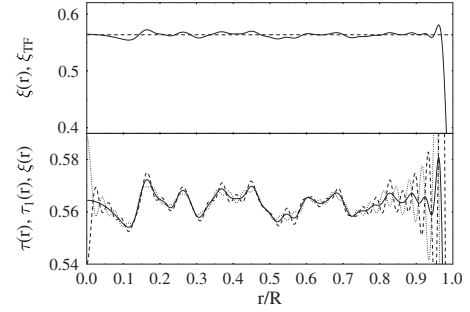

FIG. 1. Kinetic-energy density profiles of a 3D spherical billiard with $N = 100\ 068$ particles (units: $\hbar^2/2m = R = 1$; all densities are divided by $N^{5/3}$). Upper panel: $\xi(r)$ (solid line) and its constant TF value ξ_{TF} (dashed). Lower panel: $\tau(r)$ (dashed), $\tau_1(r)$ (dotted), and $\xi(r)$ (solid line). Note that in both panels, the vertical scale does not start at zero.

same two types of oscillations are also found in the particle density $\rho(r)$.

For radial systems, we can thus decompose the oscillating parts of the spatial densities defined in Eqs. (19)–(22) as follows:

$$\delta\rho(r) = \delta_r\rho(r) + \delta_{irr}\rho(r),$$
(23)

$$\delta\tau(r) = \delta_r\tau(r) + \delta_{irr}\tau(r),$$
(24)

$$\delta\tau_1(r) = \delta_r\tau_1(r) + \delta_{irr}\tau_1(r),$$
(25)

$$\delta\xi(r) = \delta_{irr}\xi(r).$$
(26)

Here the subscript "r" denotes the regular, short-ranged parts of the oscillations, while their long-ranged, irregular parts are denoted by the subscript "irr." We emphasize that this separation of the oscillating parts does not hold close to the classical turning points.

As we see in Fig. 1 and in later examples, the oscillating parts defined above fulfill the following properties in the interior of the system (i.e., except for a small region around the classical turning points):

(a) For $D > 1$, the irregular oscillating parts of $\tau(r)$ and $\tau_1(r)$ are asymptotically identical and equal to $\delta\xi(r)$,

$$\delta_{irr}\tau(r) \simeq \delta_{irr}\tau_1(r) \simeq \delta_{irr}\xi(r) = \delta\xi(r).$$
(27)

(b) The irregular oscillations are *absent* (i.e., asymptotically zero) in the densities of all potentials in $D = 1$ and, also, in isotropic harmonic oscillators (see Ref. [10]) and in linear potentials (see [28]) for arbitrary D.

(c) The regular oscillating parts of $\tau(r)$ and $\tau_1(r)$ are asymptotically equal with opposite signs

$$\delta_r\tau(r) \simeq -\delta_r\tau_1(r).$$
(28)

(This relation holds in particular for isotropic harmonic oscillators, for which it has been derived [10] asymptotically for $N \to \infty$ from quantum mechanics.)

These numerical findings will be understood and explained within the semiclassical theory developed in the following. Henceforth, the symbol δ will always denote the sum of both types of oscillating parts and the subscripts will only

be used if reference is made to one particular type of oscillations.

III. SEMICLASSICAL CLOSED-ORBIT THEORY

In this section, we present the semiclassical theory, initiated by Gutzwiller (see [29] and earlier references quoted therein and [20]), for the approximate description of quantum oscillations in terms of classical orbits. In Sec. III A, we recall the trace formula for the density of states and in Sec. III B we present the newly developed theory for spatial density oscillations [19]. In both cases, we limit ourselves—as in the previous section—to N noninteracting fermions in a local potential $V(\mathbf{r})$. The inclusion of finite temperatures in the semiclassical theory is dealt with in the Appendix.

A. Brief review of periodic orbit theory for the density of states

Before deriving semiclassical expressions for the spatial densities, we remind the reader of the periodic orbit theory (POT) for the density of states. The starting point is the semiclassical approximation of the Green's function (9) which was derived by Gutzwiller [20]

$$G_{\rm scl}(E,\mathbf{r},\mathbf{r}') = \alpha_D \sum_\gamma \sqrt{|\mathcal{D}_\gamma|}\exp\left[\frac{i}{\hbar}S_\gamma(E,\mathbf{r},\mathbf{r}') - i\mu_\gamma\frac{\pi}{2}\right]. \quad (29)$$

The sum runs over all classical trajectories γ leading from a point $\mathbf{r}$ to the point $\mathbf{r}'$ at fixed energy E. $S_\gamma(E,\mathbf{r},\mathbf{r}')$ is the action integral taken along the trajectory γ,

$$S_\gamma(E,\mathbf{r},\mathbf{r}') = \int_\mathbf{r}^{\mathbf{r}'} \mathbf{p}(E,\mathbf{q}) \cdot d\mathbf{q}, \quad (30)$$

whereby $\mathbf{p}(E,\mathbf{r})$ is the classical momentum

$$\mathbf{p}(E,\mathbf{r}) = \frac{\dot{\mathbf{r}}}{|\dot{\mathbf{r}}|}\sqrt{2m[E-V(\mathbf{r})]}, \quad (31)$$

defined only inside the classically allowed region where $E \geq V(\mathbf{r})$; its modulus is denoted by $p(E,\mathbf{r})$. $\mathcal{D}_\gamma$ is the Van Vleck determinant

$$\mathcal{D}_\gamma = \frac{(-1)^D m^2}{p(E,\mathbf{r})p(E,\mathbf{r}')}\mathcal{D}_\perp, \quad \mathcal{D}_\perp = \det(\partial\mathbf{p}_\perp/\partial\mathbf{r}'_\perp), \quad (32)$$

where $\mathbf{p}_\perp$ and $\mathbf{r}'_\perp$ are the initial momentum and final coordinate, respectively, *transverse* to the orbit γ. The Morse index μ_γ counts the sign changes of the eigenvalues of the Van Vleck determinant along the trajectory γ between the points $\mathbf{r}$ and $\mathbf{r}'$; it is equal to the number of conjugate points along the trajectory [30]. The prefactor in Eq. (29) is given by

$$\alpha_D = 2\pi(2i\pi\hbar)^{-(D+1)/2}. \quad (33)$$

The approximation (29) of the Green's function is now inserted into the right-hand side of Eq. (13) for the density of states $g(E)$. Since $\mathbf{r}' = \mathbf{r}$ in the trace integral of Eq. (13), only closed orbits contribute to it. The running time $T_\gamma(E,\mathbf{r})$ of these orbits, i.e., the time it takes the classical particle to run though the closed orbit, is given by

$$T_\gamma(E,\mathbf{r}) = \frac{dS_\gamma(E,\mathbf{r},\mathbf{r})}{dE}. \quad (34)$$

It was shown by Berry and Mount [31] that to leading order in $\hbar$, the orbits with zero running time, $T_\gamma(E,\mathbf{r})=0$, yield the smooth TF value of $g(E)$. In systems with $D > 1$, higher-order terms in $\hbar$ also contribute, which can also be obtained from the ETF model (see, e.g., chapter 4 of [26]). Separating smooth and oscillatory parts of the density of states by defining

$$g(E) := \widetilde{g}(E) + \delta g(E), \quad (35)$$

the oscillating part $\delta g(E)$ is, to leading order in $\hbar$, given by the *semiclassical trace formula*

$$\delta g(E) \simeq \sum_{\rm PO} \mathcal{A}_{\rm PO}(E)\cos\left[\frac{1}{\hbar}S_{\rm PO}(E) - \frac{\pi}{2}\sigma_{\rm PO}\right], \quad (36)$$

where the sum runs over all *periodic orbits* (POs). For systems in which all orbits are isolated in phase space, Gutzwiller [29] derived explicit expressions for the amplitudes $\mathcal{A}_{\rm PO}(E)$, which depend on the stability of the orbits, and for the Maslov indices $\sigma_{\rm PO}$. Performing the trace integral in Eq. (13) along all directions transverse to each orbit γ in the stationary-phase approximation (SPA) leads immediately to the periodicity of the contributing orbits. The Maslov index $\sigma_{\rm PO}$ collects all phases occurring in Eq. (29) and in the SPA for the trace integral (see [32] for detailed computations of $\sigma_{\rm PO}$). It has been shown [33] that $\sigma_{\rm PO}$ is a canonical and topological invariant property of any PO. $S_{\rm PO}(E)$ is the closed action integral

$$S_{\rm PO}(E) = \oint_{\rm PO} \mathbf{p}(E,\mathbf{q}) \cdot d\mathbf{q}. \quad (37)$$

For smooth one-dimensional potentials, the trace formula is particularly simple and reads

$$\delta g^{(D=1)}(E) = \frac{T_1(E)}{\pi\hbar}\sum_{k=1}^\infty (-1)^k\cos\left[\frac{k}{\hbar}S_1(E)\right], \quad (38)$$

where the sum is over the repetitions $k \geq 1$ of the primitive orbit with action $S_1(E)$ and period $T_1(E) = S_1'(E)$. Equation (38) is equivalent to the sum of delta functions in Eq. (13) using the spectrum obtained in the WKB approximation [26,34]. For systems with $D > 1$ with continuous symmetries (and hence also for integrable systems), the same type of trace formula (36) holds, but the summation includes all degenerate families of periodic orbits and the amplitudes $\mathcal{A}_{\rm PO}(E)$ and indices $\sigma_{\rm PO}$ have different forms. For an overview of various trace formulas and the pertinent literature, as well as many applications of the POT, we refer to [26].

B. Semiclassical approximation to the spatial densities

In order to derive semiclassical expressions for the spatial densities defined in Sec. II, we start from the expressions given in the Eqs. (10)–(12), which are functions of $\mathbf{r}$ and the Fermi energy λ, and replace the exact Green's function $G(E,\mathbf{r},\mathbf{r}')$ by its semiclassical expansion (29). The energy

integration can be done by parts, using Eqs. (32) and (34), and to leading order in $\hbar$ we obtain for the particle density

$$
\rho(\lambda,\mathbf{r}) \simeq \frac{2m\hbar}{\pi p(\lambda,\mathbf{r})} \mathrm{Re}\ \alpha_D \sum_\gamma \frac{\sqrt{|\mathcal{D}_\perp|}|_{\mathbf{r}'=\mathbf{r}}}{T_\gamma(\lambda,\mathbf{r})} \exp\left[\frac{i}{\hbar} S_\gamma(\lambda,\mathbf{r},\mathbf{r}) \right.
$$
$$
\left. - i\mu_\gamma \frac{\pi}{2} \right]. \tag{39}
$$

Again, the orbits with zero running time $T(E,\mathbf{r})=0$ yield, to leading order in $\hbar$, the smooth TF particle density (15); the proof given in [31] for the density of states applies also to the spatial densities discussed here. Like for the density of states, higher-order $\hbar$ corrections contribute also to the smooth part of $\rho(\mathbf{r})$ in $D>1$ and will be included in their ETF expressions. The POs, too, can only contribute to the smooth part of $\rho(\mathbf{r})$ since their action integrals (37) are independent of $\mathbf{r}$ and hence the phase in the exponent of Eq. (39) is constant. Thus, *a priori* only *nonperiodic orbits* (NPOs) contribute to the oscillating part of $\rho(\mathbf{r})$. The same holds also for the other spatial densities so that we can write their semiclassical approximations as [19]

$$
\delta\rho(\mathbf{r}) \simeq \frac{2m\hbar}{\pi p(\widetilde{\lambda},\mathbf{r})} \mathrm{Re}\ \alpha_D \sum_{\mathrm{NPO}} \frac{\sqrt{|\mathcal{D}_\perp|}|_{\mathbf{r}'=\mathbf{r}}}{T(\widetilde{\lambda},\mathbf{r})} \exp[i\Phi(\widetilde{\lambda},\mathbf{r})],
\tag{40}
$$

$$
\delta\tau(\mathbf{r}) \simeq \frac{\hbar p(\widetilde{\lambda},\mathbf{r})}{\pi} \mathrm{Re}\ \alpha_D \sum_{\mathrm{NPO}} \frac{\sqrt{|\mathcal{D}_\perp|}|_{\mathbf{r}'=\mathbf{r}}}{T(\widetilde{\lambda},\mathbf{r})} \exp[i\Phi(\widetilde{\lambda},\mathbf{r})],
\tag{41}
$$

$\delta\tau_1(\mathbf{r})$

$$
\simeq \frac{\hbar p(\widetilde{\lambda},\mathbf{r})}{\pi} \mathrm{Re}\ \alpha_D \sum_{\mathrm{NPO}} Q(\widetilde{\lambda},\mathbf{r}) \frac{\sqrt{|\mathcal{D}_\perp|}|\mathbf{r}'=\mathbf{r}}{T(\widetilde{\lambda},\mathbf{r})} \exp[i\Phi(\widetilde{\lambda},\mathbf{r})].
\tag{42}
$$

The sums are only over NPOs that lead from a point $\mathbf{r}$ back to the same point $\mathbf{r}$. For convenience, we have omitted the subscript "NPO" from all quantities in the above equations. The phase function $\Phi(\widetilde{\lambda},\mathbf{r})$ is given by

$$
\Phi(\widetilde{\lambda},\mathbf{r}) = S(\widetilde{\lambda},\mathbf{r},\mathbf{r})/\hbar - \mu\frac{\pi}{2}.
\tag{43}
$$

The quantity $Q(\widetilde{\lambda},\mathbf{r})$ appearing in Eq. (42) for $\delta\tau_1(\mathbf{r})$ is defined as

$$
Q(\widetilde{\lambda},\mathbf{r}) = \frac{[\mathbf{p}(\widetilde{\lambda},\mathbf{r}) \cdot \mathbf{p}(\widetilde{\lambda},\mathbf{r}')]_{\mathbf{r}'=\mathbf{r}}}{p^2(\widetilde{\lambda},\mathbf{r})} = \cos[\theta(\mathbf{p},\mathbf{p}')], \tag{44}
$$

where $\mathbf{p}$ and $\mathbf{p}'$ are the short notations for the initial and final momenta, respectively, of a given closed orbit γ at the point $\mathbf{r}$. These are obtained also from the action integral (30) by the canonical relations

$$
\nabla_\mathbf{r} S_\gamma(\widetilde{\lambda},\mathbf{r},\mathbf{r}')|_{\mathbf{r}=\mathbf{r}'} = -\mathbf{p}, \quad \nabla_{\mathbf{r}'} S_\gamma(\widetilde{\lambda},\mathbf{r},\mathbf{r}')|_{\mathbf{r}=\mathbf{r}'} = \mathbf{p}'. \tag{45}
$$

Since Q in Eq. (44) depends on the angle θ between $\mathbf{p}$ and $\mathbf{p}'$, it may be called the "momentum mismatch function," being $+1$ for $\mathbf{p}=\mathbf{p}'$ (i.e., for POs) and -1 for $\mathbf{p}=-\mathbf{p}'$ (e.g., for self-retracing NPOs).

Note that the upper limit λ of the energy integral in Eqs. (10)–(12) has been replaced here by the smooth Fermi energy $\widetilde{\lambda}$ defined by

$$
N = 2\int_0^{\widetilde{\lambda}} dE\widetilde{g}(E), \quad \lambda = \widetilde{\lambda} + \delta\lambda. \tag{46}
$$

The reason for this is the following. Since $\lambda(N)$ is a non-smooth staircase function, as mentioned at the end of Sec. II, it is natural to expand it around its smooth part $\widetilde{\lambda}$ which can be identified with its TF value λ_{TF} (or λ_{ETF} for $D>1$). Taylor expanding Eq. (14) using Eq. (35) up to first order in $\delta\lambda$, we easily obtain an expression for its oscillating part (cf. [35])

$$
\delta\lambda \simeq -\frac{1}{g_{\mathrm{ETF}}(\widetilde{\lambda})} \int_0^{\widetilde{\lambda}} dE \delta g(E). \tag{47}
$$

The quantity $\delta\lambda$ is of higher order in $\hbar$ than $\widetilde{\lambda}$ and can be considered as a small semiclassical correction; the $\delta g(E)$ in the integrand may be expressed through the trace formula (36). Now, the contribution of the zero-length orbits to Eq. (39) yields formally the smooth (E)TF density, but taken at the exact (quantum) value of λ. The density should therefore be developed around the smooth (E)TF value $\widetilde{\lambda}$ before it can be identified with the standard (E)TF density. Its first variation with $\delta\lambda$ leads to a further smooth contribution which should be taken into account. The same holds for the other densities. The contribution of all finite-length orbits to (39) is of higher order in $\hbar$ than the leading smooth (ETF) terms so it is consistent to evaluate them at $\widetilde{\lambda}$.

In one-dimensional systems, all smooth terms can be exactly controlled. The smooth part of the density may be written as

$$
\rho_{\mathrm{TF}}(\lambda,x) \simeq \rho_{\mathrm{TF}}(\widetilde{\lambda},x) + \delta\lambda \frac{d\rho_{\mathrm{TF}}(\lambda,x)}{d\lambda}\bigg|_{\widetilde{\lambda}}. \tag{48}
$$

The first term on the right-hand side is the standard TF density (for $D=1$). The second term, using Eq. (38) and the fact that $g_{\mathrm{TF}}(\lambda_{\mathrm{TF}})=T_1(\lambda_{\mathrm{TF}})/2\pi\hbar$ for $D=1$, is found to exactly cancel the contribution of the periodic orbits to Eq. (39) (evaluated at $\widetilde{\lambda}$), which has been explicitly calculated in [19] and given in Eq. (22) there.

For $D>1$ dimensions, we cannot prove that the same cancellation of smooth terms takes place. Furthermore, for the circular billiard treated in [21], it is shown that the contributions of periodic and nonperiodic orbits cannot be separated in the vicinity of bifurcations that occur for $D>1$ under variation of $\mathbf{r}$. For arbitrary local potentials in $D>1$ dimensions, it is in general a difficult task to evaluate all nonperiodic closed orbits. In nonintegrable systems, the number of POs is known to grow exponentially with energy or some other chaoticity parameter (cf. the Appendix H in [36] or, to

a large extent, [37]); the number of NPOs is evidently even much larger.

For the semiclassical density of states (36), the summation over POs is known not to converge in general (cf. [38]). For the semiclassical expressions (40)–(42), however, the convergence of the sums over NPOs is appreciably improved due to the appearance of their periods $T(\widetilde{\lambda}, \mathbf{r})$ in the denominators. In practice, we find that it is sufficient to include only a finite number of shortest orbits, as illustrated, for example, in Fig. 5 below.

The expressions (40)–(42) are only valid if the NPOs going through a given point $\mathbf{r}$ are *isolated*. In systems with continuous symmetries, *caustic points* exist in which the Van Vleck determinant $\mathcal{D}_\perp$ becomes singular. The same happens at points where *bifurcations* of NPOs occur. In such cases, *uniform approximations* can be developed which lead to finite semiclassical expressions; these will be presented in Sec. III E 3 and in [21].

We should also emphasize that the semiclassical approximations are not valid in regions close to the classical turning points $\mathbf{r}_\lambda$ defined by $V(\mathbf{r}_\lambda) = \widetilde{\lambda}$. Since the classical momentum $p(\widetilde{\lambda}, \mathbf{r}_\lambda)$ in Eq. (31) becomes zero there, the spatial density (40) always diverges at the turning points. Furthermore, the running time $T(\widetilde{\lambda}, \mathbf{r})$, which appears in the denominator of all densities (40)–(42), may turn to zero at the turning point for certain orbits. To remedy these divergences, one has to resort to the technique of linearizing a smooth potential $V(\mathbf{r})$ around the classical turning points, which is familiar from WKB theory [39]. We shall discuss this in detail in Sec. IV.

Our semiclassical formulas (40)–(42) can also be applied to billiard systems in which a particle moves freely inside a given domain and is ideally reflected at its boundary. The only modification is that for a given orbit, each reflection at the boundary contributes one extra unit to the Morse index μ in Eq. (43) since the difference in the semiclassical reflection phases between a soft and a hard wall is $\pi/2$. A detailed application of our formalism to the two-dimensional circular billiard, including a complete determination of all closed orbits of this system, has been given in [21].

C. Local virial theorem

Statement and test of the theorem

We now shall discuss a result which can be directly inferred from the semiclassical Eqs. (40)–(42), without detailed knowledge of the NPOs that contribute to them in a particular potential. Since the modulus of the momentum $p(\widetilde{\lambda}, \mathbf{r})$ depends only on position and Fermi energy, but not on the orbits, we have taken it outside the sum over the NPOs. Comparing the prefactors in Eqs. (40) and (41) and using Eq. (31), we immediately find [19] the relation

$$\delta\tau(\mathbf{r}) \simeq [\widetilde{\lambda} - V(\mathbf{r})]\delta\rho(\mathbf{r}). \qquad (49)$$

This is exactly the local virial theorem (LVT) that was derived in [10] from the quantum-mechanical densities in the asymptotic limit $N \to \infty$ for isotropic harmonic oscillators. Here we obtain it explicitly from our semiclassical approxi-
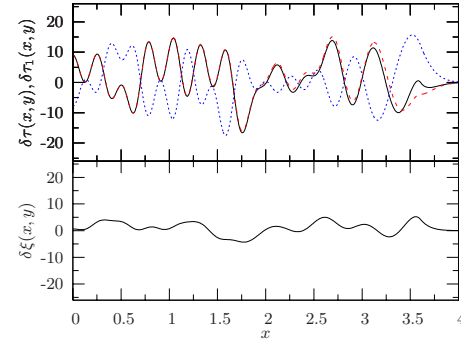

FIG. 2. (Color online) Oscillating part of spatial densities of $N = 632$ particles in the nearly chaotic potential (50) with $\kappa = 0.6$ ($\hbar = m = 1$). (Top) Solid (black) line gives the right-hand side of the LVT (49), the dashed (red) line gives $\delta\tau(x, y)$, and the dotted (blue) line gives $\delta\tau_1(x, y)$, all taken along the line $y = x/\sqrt{3}$. (Bottom) $\delta\xi(x, y)$ along $y = x/\sqrt{3}$.

mation. Since no further assumption about the potential or the contributing NPOs has been made, the LVT (49) holds for arbitrary integrable or nonintegrable systems in arbitrary dimensions with local potentials $V(\mathbf{r})$ and hence also for *interacting fermions in the mean-field approximation given by the DFT*. We recall, however, that Eq. (49) is not expected to be valid close to the classical turning points.

No such theorem holds for the density $\delta\tau_1(\mathbf{r})$ since it depends on the relative directions of the momenta $\mathbf{p}$ and $\mathbf{p}'$ of each contributing orbit through the factor $Q(\widetilde{\lambda}, \mathbf{r})$ (44) appearing under the sum in Eq. (42). In Fig. 2 we test Eq. (49) explicitly for the coupled two-dimensional quartic oscillator

$$V(x, y) = \frac{1}{2}(x^4 + y^4) - \kappa x^2 y^2, \qquad (50)$$

whose classical dynamics is almost chaotic in the limits $\kappa = 1$ and $\kappa \to -\infty$ [40,41], but in practice also for $\kappa = 0.6$ (see, e.g., [42]). We have computed its wave functions using the code developed in [42]. In the upper panel of Fig. 2, we show the left side (dashed line) and the right side (solid line) of the LVT (49) for this system with $N = 632$ particles, using the exact densities along line $y = x/\sqrt{3}$, i.e., $\delta\rho(x, x/\sqrt{3})$ and $\delta\tau(x, x/\sqrt{3})$. The agreement between both sides is seen to be very good, except in the surface region. We also show $\delta\tau_1(x, x/\sqrt{3})$ (dotted line). This demonstrates that the leading contributing NPOs in this system are not self-retracing. Correspondingly, the quantity $\delta\xi(x, x/\sqrt{3})$ in the lower panel is seen not to be negligible.

D. $D = 1$ dimensional systems

In a one-dimensional potential $V(x)$, there is only linear motion along the x axis. As discussed in [19], the only types of NPOs are those running from a given point x to one of the turning points and back, including $k \geq 0$ full periodic oscillations between both turning points. We name the two types of orbits the "+" orbits that start from any point $x \neq 0$ toward the *closest* turning point and return to x and the "−" orbits that are first reflected from the *farthest* turning point. Clearly, these orbits have opposite initial and final momenta, $p = -p'$,
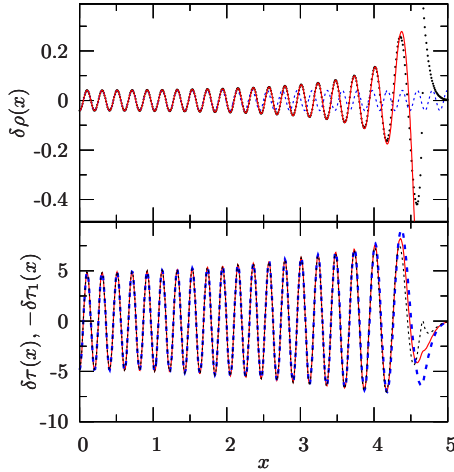
FIG. 3. (Color online) (Upper panel) Oscillating part $\delta\rho(x)$ of the particle density of $N=40$ particles in the quartic potential (53) (without spin degeneracy; units: $\hbar=m=1$). Dots (black) show the quantum-mechanical result; solid line (red) shows the semiclassical result (52) and dashed line (blue) the approximation (65) (for $D=1$) valid for small x values. (Lower panel) Tests of relations (49) and (51) between the quantum-mechanical densities for the same system. Solid line (red): $\delta\tau(x)$, dashed line (blue): $-\delta\tau_1(x)$, dotted line (black): right-hand side of Eq. (49). (Corrected figure from [19].)

so that the momentum mismatch function (44) equals $Q(\widetilde{\lambda},x)=-1$. Consequently, one obtains from Eq. (42) directly the relations

$$\delta\tau_1(x) \simeq -\delta\tau(x), \quad \delta\xi(x) \simeq 0. \quad (51)$$

Note that these results do not hold near the classical turning points, where the semiclassical approximation breaks down (cf. Sec. IV; see also the example in Fig. 10, where $\delta\xi(x)$ is small inside the systems but becomes comparable to $\delta\rho(x)$ near the turning points).

The explicit evaluation of Eq. (40) for $D=1$ was done in [19] for smooth potentials; the result in the present notation is

$$\delta\rho(x) \simeq -\frac{m}{\pi p(\widetilde{\lambda},x)} \sum_{k=0,\pm}^{\infty} (-1)^k \frac{\cos[kS_{\pm}^{(k)}(\widetilde{\lambda},x)/\hbar]}{T_{\pm}^{(k)}(\widetilde{\lambda},x)}, \quad (52)$$

where $S_{\pm}^{(k)}$ are the actions of the "+" and "−"-type NPOs (including k full periods) and $T_{\pm}^{(k)}$ are there running times defined by Eq. (34).

A numerical example was given in [19] for the quartic oscillator in one dimension

$$V(x) = x^4/4. \quad (53)$$

Unfortunately, an error occurred in the drawing of Fig. 1 in [19]; the present Fig. 3 is its corrected version. In the upper panel, it is seen that the semiclassical approximation (52) for $\delta\rho(x)$ agrees very well with the quantum result and in the lower panel, the relations (49) and (51) between the quantum results are seen to be well fulfilled. The only sizable deviations occur very near the classical turning point, as expected.

We emphasize that the Friedel oscillations near the surface are dominated by the primitive + orbit (with $k=0$). Its contribution diverges, however, since its running time $T_+^{(0)}(\widetilde{\lambda},x)$ tends to zero there. This divergence can be remedied in the WKB-type linear approximation to the potential which we discuss in Sec. IV A for smooth potentials or by the short-time propagator for hard-wall potentials (i.e., billiard systems) discussed in Sec. IV B. First we will, however, examine the strictly linear potential for which the WKB approximation is exact.

1. Linear potential

In [28], we give the exact quantum-mechanical densities for the one-dimensional potential $V(x)=ax$. Although this potential does not bind any particles, its density close to the turning point will be of use in Sec. IV A. Here we give its semiclassical analysis.

Since a particle cannot be bound in this potential, the only closed classical orbit starting from a point x is the primitive orbit + ($k=0$) going to the turning point $x_\lambda=\widetilde{\lambda}/a$ and back to x. Its action is

$$S_+(x) = S_+^{(0)}(x) = 2\int_x^{x_\lambda} p(\widetilde{\lambda},x)dx = \frac{4\sqrt{2m}}{3a}(\widetilde{\lambda}-ax)^{3/2}$$

$$= \hbar\frac{4}{3}|z_\lambda|^{3/2} = \hbar 2\zeta_\lambda, \quad (54)$$

where the last equalities make use of the quantities defined as

$$\sigma = \left(\frac{2m}{\hbar^2 a^2}\right)^{1/3} \quad (55)$$

and

$$z_\lambda = \sigma(ax-\lambda), \quad \rho_0 = 2\left(\frac{2ma}{\hbar^2}\right)^{1/3} = 2\sigma a. \quad (56)$$

Using Eq. (40) for $D=1$, we obtain the semiclassical contribution of this orbit to the spatial density [cf. Eq. (23) of [19] with $\sigma=+$, $k=1$]

$$\delta\rho(x) = -\frac{a}{2\pi}\frac{1}{(\widetilde{\lambda}-ax)}\cos\left[\frac{1}{\hbar}S_+(x)\right], \quad (57)$$

which is identical to the asymptotic expression for the exact quantum-mechanical result [28]. Thus, the orbit + creates the Friedel oscillations. Using the LVT (49) and $Q=-1$ in Eq. (42), we obtain immediately the expression for the kinetic-energy densities

$$\delta\tau(x) = -\delta\tau_1(x) = -\frac{a}{2\pi}\cos\left[\frac{1}{\hbar}S_+(x)\right], \quad (58)$$

which is identical to the asymptotic quantum result [28]. The expression (57) diverges at the classical turning point x_λ. To avoid this divergence, one has to use the exact expressions [28], which can be considered as the regularized contributions of the primitive + orbit near the turning points.

2. One-dimensional box

For the one-dimensional box of length L, Eq. (52) has to be modified by omitting the phase factor $(-1)^k$, since each turning point gives two units to the Morse index. Using $\rho_{\text{TF}} = 2/\pi\sqrt{2m\lambda_{\text{TF}}/\hbar^2}$ and summing over all k, one finds that it reproduces exactly the quantum-mechanical $\rho(x)$ in the large-N limit so that the semiclassical approximation here is asymptotically exact.

E. $D > 1$ dimensional potentials with spherical symmetry

In this section, we discuss potentials in $D > 1$ with spherical symmetry so that $V(\mathbf{r}) = V(r)$ depends only on the radial variable $r = |\mathbf{r}|$. The particle number N is chosen such that energy levels with angular-momentum degeneracy are filled so that all spatial densities, too, depend only on r. In such systems, the two kinds of oscillations discussed in Sec. II B 2 can always be separated clearly in the central region $r \simeq 0$. Indeed, this behavior is explained by the fact that the angular momentum of the orbits is conserved. Therefore, the shape of a closed orbit whose starting point r approaches the center of the potential tends to become flattened and concentrated near a radial periodic orbit. Thus, close to the center, there are only two types of nonperiodic orbits. First, the *radial* orbits of the same types $+$ and $-$ as discussed for the one-dimensional case, with opposite momenta $\mathbf{p} = -\mathbf{p}'$, leading to the same kind of oscillations that we know for $D = 1$. Second, *nonradial* orbits which near $r = 0$ have almost equal momenta $\mathbf{p} \simeq \mathbf{p}'$ so that they become nearly periodic.

Semiclassically, the two types of radial and nonradial NPOs are responsible precisely for the two kinds of oscillations which we described in Sec. II B 2. The regular short-ranged oscillations, denoted $\delta_r\rho(r)$, etc., can be attributed to the radial $+$ and $-$ orbits. The long-ranged irregular oscillations, denoted $\delta_{\text{irr}}\rho(r)$, etc., must be attributed to the nonradial NPOs: these lead to slow oscillations because their actions are almost independent of the starting point near $r = 0$.

The contributions of the radial NPOs in radially symmetric systems have already been anticipated in [19]; they will be discussed in the following section. In particular, like for $D = 1$, the primitive $+$ orbit is seen to be solely responsible for the Friedel oscillations near the surface of a $D > 1$ dimensional spherical system.

Nonradial orbits can only occur if there exist classical trajectories which intersect themselves in a given point $\mathbf{r}$. As is well known from classical mechanics, such orbits do not exist in isotropic harmonic oscillators (and in the Coulomb potential). This explains the fact that no irregular long-ranged oscillations are found in the densities of harmonic oscillators [10] (or, trivially, in any one-dimensional potential).

We emphasize that for $D = 2$, all closed NPOs are isolated except if they start at $r = 0$, in which case they form degenerate families due to the radial symmetry (cf. Sec. III E 3). In $D > 2$ dimensions, however, also the nonradial NPOs starting at $r > 0$ have continuous rotational degeneracies. For the corresponding families of orbits, the Van Vleck determinant $\mathcal{D}_\gamma$ in the semiclassical Green's function (29) becomes singular at all points r. This divergence can be removed [43] by going

one step back in the derivation of Eq. (29). In the convolution integral for the time-dependent propagator, one has to perform a sufficient number of intermediate integrals exactly rather than in the stationary-phase approximation (for details, see [43] where this was done to obtain the trace formula (36) for systems with continuous symmetries). As a result, the semiclassical amplitudes of the degenerate families of orbits are of lower order in $\hbar$ than for isolated orbits and thus have a larger weight. In our present case, the $\hbar$ dependence of the ratio of amplitudes between the irregular and the regular oscillations, e.g., in the particle density, becomes

$$\frac{|\delta_{\text{irr}}\rho(r)|}{|\delta_r\rho(r)|} \propto \hbar^{-(D-2)/2}, \quad (D > 1). \tag{59}$$

The same ratio holds also for the other spatial densities. This can be seen, e.g., in Fig. 1 for the spherical billiard in $D = 3$, where the amplitude of the irregular oscillations is larger than that of the radial oscillations (except near $r = 0$). In passing, we note that for spherical billiards with radius R, the energy dependence of the semiclassical results scales with the dimensionless variable $p_\lambda R/\hbar$ and the ratio (59) becomes $|\delta_{\text{irr}}\rho / \delta_r\rho| \propto [p_\lambda R/\hbar]^{(D-2)/2}$.

It should be stressed that the separation of two classes of NPOs and hence the two types of oscillations is not possible in systems in $D > 1$ dimensions without radial symmetry. This will be illustrated in Sec. III F.

A further complication in systems with $D > 1$ is that the NPOs can undergo bifurcations under the variation of the starting point r. At these bifurcations, new NPOs or POs are created. This is discussed extensively in a publication [21] on the two-dimensional circular billiard. For this system, a complete classification of all NPOs could be made and analytical expressions for their actions and Van Vleck determinants have been derived.

1. Contributions of the radial orbits: Earlier results

Recall that since all radial NPOs fulfill $\mathbf{p}' = -\mathbf{p}$, they have $Q(\tilde{\lambda}, r) = -1$ under the sum in Eq. (42). Therefore, we immediately obtain the semiclassical relation [19]

$$\delta_r\tau_1(r) \simeq -\delta_r\tau(r). \tag{60}$$

Indeed, this was found to be fulfilled, sufficiently far from the turning point, for all quantum systems with radial symmetry that we have studied numerically.

For the following, it is important to notice the action of the differential operator ∇ on the semiclassical density in Eq. (40). The contributions of leading order in $\hbar$ (i.e., the terms of the largest *negative* power of $\hbar$) come from the phase $\Phi(\tilde{\lambda}, \mathbf{r})$ given in Eq. (43). From the canonical relations (45), we find

$$\nabla \exp[i\Phi(\tilde{\lambda}, \mathbf{r})] = \frac{i}{\hbar}(\mathbf{p}' - \mathbf{p})\exp[i\Phi(\tilde{\lambda}, \mathbf{r})] \tag{61}$$

and

$$\nabla^2 \exp[i\Phi(\widetilde{\lambda}, \mathbf{r})] = -\frac{1}{\hbar^2}(\mathbf{p}' - \mathbf{p})^2 \exp[i\Phi(\widetilde{\lambda}, \mathbf{r})], \quad (62)$$

which occurs for each NPO under the summation in Eq. (40). For the radial orbits, one therefore obtains with Eq. (31) the following differential equation for $\delta_r\rho(r)$, which was already given in [10]:

$$-\frac{\hbar^2}{8m}\nabla^2 \delta_r\rho(r) \simeq [\widetilde{\lambda} - V(r)]\delta_r\rho(r). \quad (63)$$

For small distances r from the center so that $V(r) \ll \widetilde{\lambda}$, Eq. (63) becomes the universal Laplace equation

$$-\frac{\hbar^2}{8m}\nabla^2 \delta_r\rho(r) \simeq \widetilde{\lambda}\delta_r\rho(r), \quad (64)$$

which was obtained asymptotically from the quantum-mechanical densities of isotropic harmonic oscillators in [10]. It has the general solution

$$\delta_r\rho(r) = (-1)^{M_s-1}\frac{m}{\hbar T_{r1}(\widetilde{\lambda})}\left(\frac{p_\lambda}{4\pi\hbar r}\right)^\nu J_\nu(2rp_\lambda/\hbar). \quad (65)$$

Here, $J_\nu(z)$ is a Bessel function with index $\nu = D/2 - 1$, $M_s = M + 1$ is the number of filled main shells [44], T_{r1} is the period of the primitive radial full oscillation, and $p_\lambda = (2m\widetilde{\lambda})^{1/2}$ is the Fermi momentum. The normalization of Eq. (65) cannot be obtained from the linear Eq. (64); we have determined it from the calculation presented in Sec. III E 3. For harmonic oscillators, where $T_{r1} = 2\pi/\omega$, Eq. (65) becomes identical with the result in Eq. (69) of [10] that was derived from quantum mechanics in the large-N limit.

The quantity $\delta_r\rho(r)$ can also be calculated directly from Eq. (40), including only the radial NPOs. The summation over their repetitions goes exactly like in the one-dimensional case done in [19], except for the evaluation of the determinant $\mathcal{D}_\perp$. This determinant becomes singular at $r = 0$ due to the continuous degeneracy of the + and − orbits: the point $r = 0$ is a caustic point for all radially symmetric systems with $D > 1$. The regularization of this singularity, leading precisely to the result (65), is discussed in Sec. III E 3 below.

2. Isotropic harmonic oscillators in D dimensions

We now investigate the densities in the isotropic harmonic-oscillator (IHO) potential in D dimensions defined as

$$V(r) = \frac{m}{2}\omega^2 r^2, \quad r = |\mathbf{r}|, \quad \mathbf{r} \in \mathbb{R}^D. \quad (66)$$

First we mention the well-known fact that in IHO potentials with arbitrary $D > 1$, all orbits with nonzero angular momentum are periodic, forming ellipses which may degenerate to circles or radial librations. Hence, the only NPOs are the radial orbits + and −. Since we just have seen that in the leading-order semiclassical approximation, $\delta_r\tau_1(r) = -\delta_r\tau(r)$, it follows that $\delta\xi(r) = 0$ to leading order like for $D = 1$, thus explaining the smooth behavior of $\xi(r)$ for IHOs [10].
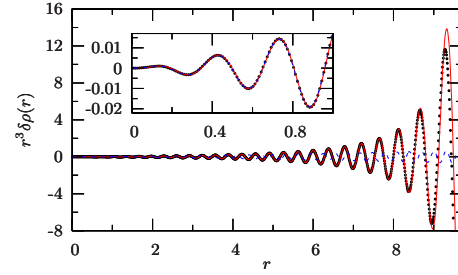

FIG. 4. (Color online) Oscillating part of the spatial particle density times r^3 for four-dimensional (4D) IHO for $N = 632\,502$, i.e., with $M = 50$ filled shells (units: $\hbar = m = \omega = 1$). Dots are the quantum results. Solid (red) line is the analytical expression (68) using the Morse indices given in Eq. (71) and dashed (blue) line is the asymptotic formula (65) valid close to $r = 0$.

For the IHO potentials, the transverse determinant $\mathcal{D}_\perp$ can be easily computed. It is diagonal and reads

$$|\mathcal{D}_\perp(\widetilde{\lambda}, r)| = \left[\frac{m\widetilde{\lambda}}{rp(\widetilde{\lambda}, r)}\right]^{D-1}, \quad (67)$$

which does not depend on the type and the repetition number k of the orbit. Following Eq. (40) and [19], we compute $\delta\rho(r)$ as a sum over the contributions of the + and − orbits, which is given by

$$\delta\rho(r) = \frac{4m\hbar}{(2\pi\hbar)^{(D+1)/2}}\frac{1}{p(\widetilde{\lambda}, r)}\left[\frac{m\widetilde{\lambda}}{rp(\widetilde{\lambda}, r)}\right]^{(D-1)/2}$$
$$\times \sum_{k=0,\pm}^\infty \frac{\cos\left[S_\pm^{(k)}(\widetilde{\lambda}, r) - (D+1)\frac{\pi}{4} - \mu_\pm^{(k)}\frac{\pi}{2}\right]}{T_\pm^{(k)}(\widetilde{\lambda}, r)}. \quad (68)$$

Here we have used the analytical form of the actions and periods

$$S_\pm^{(k)}(\widetilde{\lambda}, r) = (2k+1)\frac{\pi\widetilde{\lambda}}{\omega} \mp rp(\widetilde{\lambda}, r) \mp \frac{2\widetilde{\lambda}}{\omega}\arcsin\left(\frac{m\omega r}{p_\lambda}\right),$$
$$(69)$$

$$T_\pm^{(k)}(\widetilde{\lambda}, r) = (2k+1)\frac{\pi}{\omega} \mp \frac{2}{\omega}\arcsin\left(\frac{m\omega r}{p_\lambda}\right). \quad (70)$$

We compute the Morse indices following Gutzwiller [45]. Each turning point contributes a phase of $\pi/2$. Besides, we evaluate the number of extra conjugate points including their multiplicities depending on the dimension, contributing a phase $\pi(D-1)/2$ each (they are most easily determined from the propagator of the harmonic oscillator in the time representation). The final result for the Morse indices is

$$\mu_+^{(k)} = 2kD + 1, \quad \mu_-^{(k)} = 2kD + D. \quad (71)$$

We note that the Eq. (68) is consistent with results derived in [11] from the quantum-mechanical density $\rho(r)$.

Figure 4 shows a comparison of the semiclassical results (68) to the exact quantum result for the case $D = 4$. We have multiplied both by a factor r^3 since the semiclassical determinant $\mathcal{D}_\perp$ diverges at $r = 0$ which is a caustic point due to

the spherical symmetry. This divergence will be regularized in the following section.

Using the Morse indices (71) and the expression $\widetilde{\lambda} = \hbar\omega[M + (D+1)/2]$ [10], we can perform the summation over k in Eq. (68) analytically for small r, like it was done in [19] for the one-dimensional (1D) case. The result then is exactly that given in Eq. (65) with $T_{r1}(\widetilde{\lambda}) = 2\pi/\omega$, but replacing the Bessel function $J_\nu(z)$ by its asymptotic expression for large argument z, i.e., using

$$J_\nu(z) \rightarrow \sqrt{\frac{2}{\pi z}} \cos(z - \nu\pi/2 - \pi/4). \tag{72}$$

3. Regularization close to the center

In this section, we compute the contribution of radial NPOs to the semiclassical particle density close to the center of an arbitrary potential with radial symmetry. As stressed in the last section, the semiclassical Green's function for $D > 1$ is not defined at $r = 0$ where $\mathcal{D}_\perp$ diverges. The reason is the caustic that occurs there: fixing the position of the point $r = r' = 0$ does not uniquely determine a closed orbit (periodic or nonperiodic) which belongs to a continuously degenerate family due to the spherical symmetry. A standard method to solve this problem is to introduce the mixed phase-space representation of the Green's function close to the diverging point, as proposed initially by Maslov and Fedoriuk [46].

Here we follow more specifically the procedure outlined in [47]. The mixed representation of the Green's function can be approximated in a form analogous to that in the coordinate representation. This is due to the smoothness of the phase-space torus which implies that no diverging points can occur simultaneously in position and momentum (cf. [46]). Following Gutzwiller, we use for every classical trajectory γ an "intrinsic" (or local) coordinate system $\mathbf{r} = (r_\parallel, \mathbf{r}_\perp)$, where the coordinate $r_\parallel$ is taken along the trajectory and $\mathbf{r}_\perp$ is the vector of all other coordinates transverse to it; $\mathbf{p} = (p_\parallel, \mathbf{p}_\perp)$ is the corresponding system for the momentum. We next rewrite the coordinate representation of the Green's function as the inverse Fourier transform of the mixed Green's function with respect to the final transverse momentum $\mathbf{p}'_\perp$,

$$G_{\mathrm{scl}}(E, \mathbf{r}, r'_\parallel, \mathbf{r}'_\perp) = \frac{1}{(-2i\pi\hbar)^{(D-1)/2}} \sum_\gamma \int d\mathbf{p}'_\perp$$
$$\times \hat{G}_y(E, \mathbf{r}, r'_\parallel, \mathbf{p}'_\perp) \exp\left(\frac{i}{\hbar} \mathbf{r}'_\perp \cdot \mathbf{p}'_\perp\right), \tag{73}$$

where the sum is over all classical trajectories γ starting at $\mathbf{r}$ and ending at $(r'_\parallel, \mathbf{p}'_\perp)$ in phase space. Hereby, the contribution of the orbit γ to the semiclassical mixed representation of the Green's function is given by [46]

$$\hat{G}_y(E, \mathbf{r}, r'_\parallel, \mathbf{p}'_\perp) = \alpha_D \hat{\mathcal{D}}_y(E, \mathbf{r}, r'_\parallel, \mathbf{p}'_\perp) \exp\left(\frac{i}{\hbar} \hat{S}_\gamma(E, \mathbf{r}, r'_\parallel, \mathbf{p}'_\perp)\right.$$
$$\left. - \frac{i\pi}{2} \hat{\mu}_y\right), \tag{74}$$

where $\hat{S}$ is the Legendre transform of the action S between the variables $\mathbf{r}'_\perp$ and $\mathbf{p}'_\perp$

$$\hat{S}_\gamma(E, \mathbf{r}, r'_\parallel, \mathbf{p}'_\perp) = S_\gamma(E, \mathbf{r}, r'_\parallel, \mathbf{r}'_\perp) - \mathbf{r}'_\perp \cdot \mathbf{p}'_\perp. \tag{75}$$

Since in the mixed-representation Green's function we have to evaluate the action $\hat{S}$ for radial orbits with *fixed* momentum close to the center, the rotational symmetry in position is removed and $\hat{G}$ is regular. The Van Vleck determinant in this representation is

$$\hat{\mathcal{D}}_y = \frac{m}{|p_\parallel p'_\parallel|^{1/2}} |\hat{\mathcal{D}}_{\perp y}|^{1/2}, \quad \hat{\mathcal{D}}_{\perp y} = \det\left(\frac{\partial \mathbf{p}_\perp}{\partial \mathbf{p}'_\perp}\right) \tag{76}$$

and the Morse index becomes

$$\hat{\mu}_\gamma = \begin{cases} \mu_\gamma, & \text{for positive eigenvalue of } \det\left(\dfrac{\partial \mathbf{r}'_\perp}{\partial \mathbf{p}'_\perp}\right) \\[2ex] \mu_\gamma + 1, & \text{for negative eigenvalue of } \det\left(\dfrac{\partial \mathbf{r}'_\perp}{\partial \mathbf{p}'_\perp}\right). \end{cases}$$

Far from singular points, the evaluation of Eq. (73) using the stationary-phase approximation (SPA) yields [48] the standard semiclassical Green's function (29).

After performing the $\hbar$ expansion and the integration over the energy similarly as in [19], the oscillating part of the particle density is given by

$$\delta\rho(\mathbf{r}) = 2\sum_\gamma \mathrm{Im}\left\{\frac{i\alpha_D\hbar}{\pi T} \int d\mathbf{p}'_\perp \hat{G}(\widetilde{\lambda}, \mathbf{r}, r_\parallel, \mathbf{p}'_\perp) \exp\left(\frac{i}{\hbar} \mathbf{r}_\perp \cdot \mathbf{p}'_\perp\right)\right\}. \tag{77}$$

Close to the center of the potential, now, we replace the nonradial NPOs by the radial ones with $\gamma = \pm$ orbits with kth repetitions. For nonperiodic orbits in the radial direction r, we have $r_\parallel = r$. We neglect the higher orders in $\mathbf{r}_\perp$, leading to the following approximations:

$$|\det(\partial\mathbf{p}_\perp/\partial\mathbf{p}'_\perp)| \approx 1,$$

$$|p_\parallel| \approx |p'_\parallel| \approx p_\parallel(\widetilde{\lambda}, \mathbf{p}'_\perp) := \sqrt{2m\widetilde{\lambda} - \mathbf{p}'^2_\perp},$$

$$(r, \mathbf{r}_\perp) \approx (r, 0),$$

$$\hat{S}^{(k)}_\pm \approx (k + 1/2)S_{r1} \mp 2rp'_\parallel,$$

$$T^{(k)}_\pm \approx (k + 1/2)T_{r1}. \tag{78}$$

Furthermore, we approximate the action S_{r1} of the primitive periodic diameter orbit by $S_{r1} \approx 2\pi\hbar[M + (D+1)/2]$. This is exact for IHOs where $S_{r1} = 2\pi\widetilde{\lambda}/\omega$ and $\widetilde{\lambda} = \hbar\omega[M + (D+1)/2]$ can be used [10]; for arbitrary radial potentials, it corresponds to a radial WKB quantization, whereby M is a "main shell" quantum number that has to be suitably chosen [44]. Also, we assume that each eigenvalue of $\det(\partial\mathbf{r}'_\perp/\partial\mathbf{p}'_\perp)$ is negative (positive) for the orbits $+$ $(-)$, leading to $\hat{\mu}^{(k)}_+ = \hat{\mu}^{(k)}_-$. This is again exact for IHOs; for other radial potentials, we have verified its validity numerically. With these approximations, the sum over the repetitions of all radial orbits can be performed exactly like in the previous section. The oscillating part of the particle density then simplifies to

$$\delta_r\rho(r) = \frac{(-1)^M m}{(2\pi\hbar)^{D-1}T_{r1}}\int d\mathbf{p}'_\perp\frac{\cos[2rp_\parallel(\widetilde{\lambda},\mathbf{p}'_\perp)/\hbar]}{p_\parallel(\widetilde{\lambda},\mathbf{p}'_\perp)}. \quad (79)$$

The integration has to be taken over half the solid angle in the $(D-1)$-dimensional transverse momentum space, avoiding a double counting of the two orbits. So it is natural to make a change of variables to dimensionless hyperspherical coordinates. Using the integral representation of the Bessel functions [49]

$$J_\nu(z) = \frac{2(z/2)^{-\nu}}{\sqrt{\pi}\,\Gamma(\nu+1/2)}\int_0^1 (1-t^2)^{\nu-1/2}\cos(zt)dt, \quad (80)$$

we obtain exactly the same result as in Eq. (65), confirming its normalization.

We stress that this regularization is only valid near the center, i.e., for $r\simeq 0$, as can be seen in the example of Fig. 4, where the result (65) is displayed by the dashed line. The reason is that for larger values of r, the approximations (78) are no longer valid. If one restricts oneself to the leading contributions of the primitive orbits + and − with $k=0$, a "global uniform" approximation can be made which interpolates smoothly between the regularized result (65) near $r=0$ and the correct semiclassical contributions obtained from Eq. (40) at larger r. This uniform approximation is derived and used in [21] for the two-dimensional (2D) circular billiard system which we briefly discuss in the following section.

4. Two-dimensional circular billiard

The two-dimensional circular billiard, which can be taken as a realistic model for quantum dots with a large number N of particles, has been investigated semiclassically in [21], where all its periodic and nonperiodic closed orbits have been classified analytically. We discuss there also the various bifurcations at specific values of the radial variable r, at which POs bifurcate from NPOs or pairs of NPOs are born. At these bifurcations, the semiclassical amplitudes in Eqs. (40)–(42) must be regularized by suitable uniform approximations. We refer to [21] for the details and reproduce here some numerical results to illustrate the quality of the semiclassical approximation.

Figure 5 shows the total particle density $\rho(r)$ for $N=606$ particles in the circular billiard. The solid line gives the quantum result, obtained from Eq. (2) using the solutions of the Schrödinger equation with Dirichlet boundary conditions, which are given in terms of cylindrical Bessel functions. The dotted line gives the semiclassical result, obtained by summing over the $\sim$30 shortest NPOs. (Hereby, we used the regularization of the radial + and − orbits at $r=0$ by Eq. (65), that of the primitive + orbit near $r=R$ by Eq. (95) given in Sec. IV B 1 below, and uniform approximations for the bifurcations of some of the nonradial NPOs as described in detail in [21].) We see that, indeed, a satisfactory approximation of the quantum density can be obtained in terms of the shortest classical orbits of this system.

In Fig. 6, we demonstrate explicitly the contributions of nonradial NPOs to the kinetic-energy densities $\tau_1(r)$ and $\xi(r)$ close to the center, calculated as in Fig. 5 but for $N=9834$ particles. We clearly see that $\delta\xi(r)$ is not smooth; its slow,
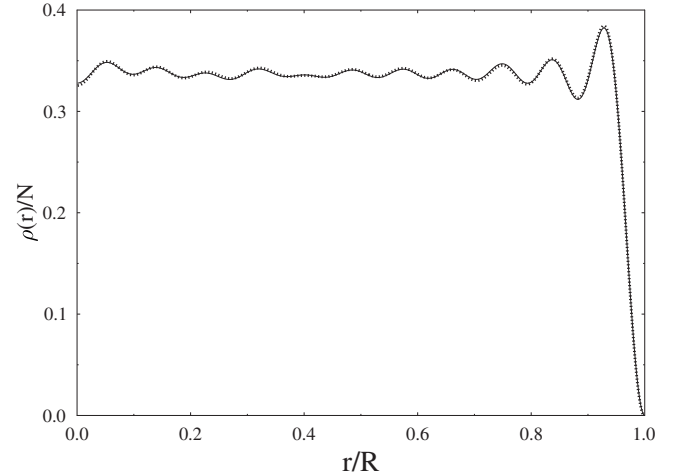

FIG. 5. Particle density in the two-dimensional disk billiard with radius R, containing $N=606$ particles (units: $\hbar^2/2m=R=1$), divided by N. Solid line is the quantum result and dotted line the semiclassical result with all regularizations (see [21] for details).

irregular oscillations are due to nonradial NPOs which have the form of polygons with $2k$ reflections ($k=1,2,\dots$) at the boundary and one corner at a point r close to the center. The first $k_{max}=20$ of them were included with the appropriate regularization at $r=0$ where they are degenerate with the kth repetitions of the diagonal PO (see [21] for details). The agreement between quantum and semiclassical results is again satisfactory; the discrepancy that sets on for $r\gtrsim 0.18$ is due to the missing of more complicated nonradial orbits. The quantity $\delta\tau_1(r)$, on the other hand, clearly exhibits both kinds of oscillations according to Eq. (25): the slow irregular part, which is identical with $\delta\xi(r)$, is modulated by the regular fast oscillations due to the radial orbits.

F. $D>1$ dimensional systems without continuous symmetries

In $D>1$ dimensional systems without continuous symmetries, it is in general not possible to find the classical orbits analytically. As in POT, the search of closed orbits must then be done numerically. A practical problem in such systems is also that the densities as functions of D coordinates are not easily displayed. For tests and comparisons of various ap-
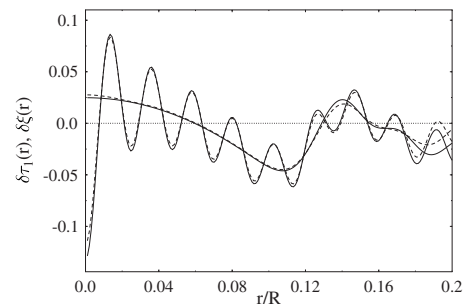

FIG. 6. Oscillating parts of kinetic-energy densities, $\delta\tau_1(r)$ (fast oscillations) and $\delta\xi(r)$ (slow oscillations) for $N=9834$, divided by $N^{5/3}$. (Solid lines) Exact quantum results. (Dashed lines) Semiclassical results and units as in Fig. 5.
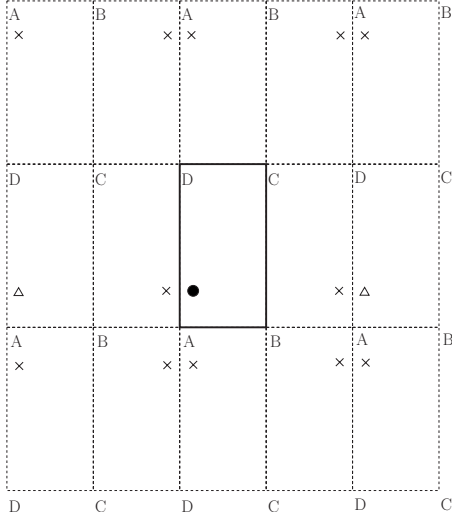
FIG. 7. Images (triangles and crosses) of a point $P(x,y)$ (full circle) for a rectangular billiard. Joining by a straight line the full circle to a cross gives a nonperiodic orbit whereas joining to a triangle gives a periodic orbit.

proximations or of the local virial theorems, we have to resort to taking suitable one-dimensional cuts (i.e., projections) of the densities. In the following paragraph, we discuss a class of integrable billiard systems, in which all closed classical orbits can easily be found and their semiclassical contributions to the densities can be analytically obtained. These are D-dimensional polygonal billiards that tessellate the full space under repeated reflections at all borders. We illustrate the method for the example of a rectangular billiard. Although this does not correspond to any physical system (unless experimentally manufactured as a rectangular quantum dot with many electrons), it is a useful model without spherical symmetry that allows for analytical calculation of the classical orbits and their properties.

Billiards tessellating flat space: The rectangular billiard

For billiards, classical trajectories are straight lines which are reflected at the boundary according to the specular law. Let us consider a two-dimensional billiard that tessellates the plane, such as the rectangular billiard shown in Fig. 7. Choose a trajectory starting at a point P, reflected at the point R_0, and reaching the point P_1. Now reflect the boundary at a

side containing the point R_0, the image R_0P_1' of the segment R_0P_1 gives the straight line PP_1'. The next portion of the trajectory after reflexion in R_1 can be found by reflecting the new billiard at the side containing R_1'. This process can be repeated until the trajectory ends. To get the closed trajectories at P, we have to compute all images of P in the images of the billiard. Now a straight line joining P and an image of P gives a closed orbit. Thus, constructing all images of P by simple geometry enables one to compute all trajectories and their related initial and final momenta for D-dimensional polygonal billiard that fills the D-dimensional Euclidean space. Note that the Jacobian $\mathcal{D}_\perp$ for these systems is easily computed and equals $(p/L_{\mathrm{NPO}})^{D-1}$, where L_{NPO} is the length of the orbit.

We illustrate this method for the case of a 2D rectangular billiard with side lengths Q_x and Q_y. There are four types of images of $P(x,y)$; one leading to POs and three (labeled by the indeces a, b, and c) leading to NPOs (see Fig. 7). Table I lists the basic ingredients to compute the spatial densities using $L(x,y)=2\sqrt{x^2+y^2}$ and

$$f(x,y,\mu) = \frac{4\hbar p_\lambda^{1/2}}{[2\pi\hbar L(x,y)]^{3/2}}\cos\left[\frac{p_\lambda L(x,y)}{\hbar} - \frac{3\pi}{4} - \mu\pi\right], \tag{81}$$

with $p_\lambda=(2m\tilde{\lambda})^{1/2}$. From Eqs. (40) and (42) for $D=2$ we obtain

$$\delta\rho(x,y) = \sum_{k_x,k_y=-\infty}^{\infty}\sum_{l=a,b,c}\delta\rho_l(x,y), \tag{82}$$

$$\delta\tau_1(x,y) = \sum_{k_x,k_y=-\infty}^{\infty}\sum_{l=a,b,c}\delta\tau_{1l}(x,y), \tag{83}$$

where the partial contributions $\delta\rho_l(x,y)$ and $\delta\tau_{1l}(x,y)$ for the orbits of types $l=a$, b, and c are given in Table I. $\delta\tau(x,y)$ is obtained from Eq. (82) using the LVT (49).

We now present numerical results for the rectangular billiard with side lengths $Q_x=2^{1/4}$, $Q_y=3^{1/4}$ (units: $\hbar^2=2m=1$), containing $N=2000$ particles. In Fig. 8, we show the quantities $\delta\rho$ (top), $\delta\tau$ (center), and $\delta\tau_1$ (bottom) as functions of y with fixed $x=Q_x/2$. Dashed lines are the quantum-mechanical results and solid lines the semiclassical ones using Eqs. (82), (83), and (49). We see that summing over all

TABLE I. Contributions of different types of nonperiodic orbits to the spatial densities in a rectangle billiard with sides Q_x and Q_y. First row gives the position of the images of P with $(k_x,k_y)\in\mathbb{Z}^2$. Second row gives the length of the orbit and third row the angle θ between the initial and final momenta. Fourth and fifth rows give the contributions to $\delta\rho$ and $\delta\tau_1$, respectively.

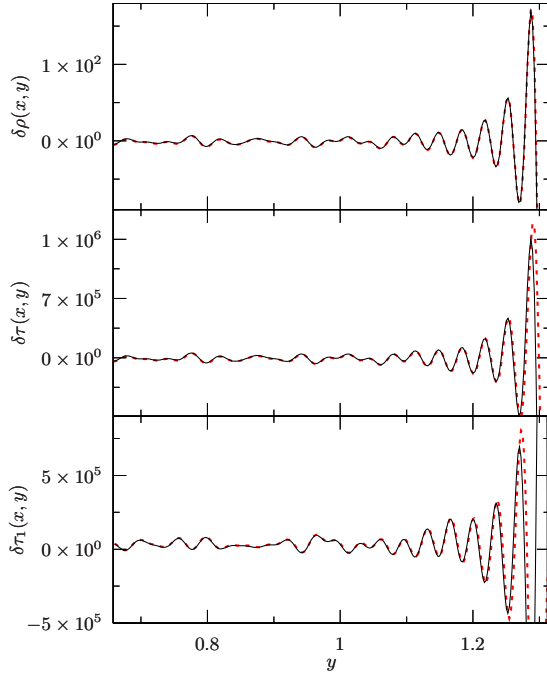| Type of orbits	a	b	c
Image points of $P(x,y)$	$(2k_xQ_x+x,2k_yQ_y-y)$	$(2k_xQ_x-x,2k_yQ_y+y)$	$(2k_xQ_x-x,2k_yQ_y-y)$
Orbit length	$L(k_xQ_x,k_yQ_y-y)$	$L(k_xQ_x-x,k_yQ_y)$	$L(k_xQ_x-x,k_yQ_y-y)$
θ	$\theta_a=-2\arctan\left(\frac{k_yQ_y-y}{k_xQ_x}\right)$	$\theta_b=2\arctan\left(\frac{k_yQ_y}{k_xQ_x-x}\right)$	$\theta_c=\pi$
Contribution to $\delta\rho$	$\delta\rho_a=f(k_xQ_x,k_yQ_y-y,1)$	$\delta\rho_b=f(k_xQ_x-x,k_yQ_y,1)$	$\delta\rho_c=f(k_xQ_x-x,k_yQ_y-y,0)$
Contribution to $\delta\tau_1$	$\delta\tau_{1a}=\tilde{\lambda}\cos(\theta_a)\delta\rho_a$	$\delta\tau_{1b}=\tilde{\lambda}\cos(\theta_b)\delta\rho_b$	$\delta\tau_{1c}=\tilde{\lambda}\cos(\theta_c)\delta\rho_c$

FIG. 8. (Color online) Oscillating part of the spatial densities for a rectangular billiard with sides $Q_x = 2^{1/4}$ and $Q_y = 3^{1/4}$ for $N = 2000$ along the line $x = Q_x/2$ (units: $\hbar^2 = 2m = 1$). Solid (black) lines are the semiclassical results using Eqs. (82), (83), and (49); dashed (red) lines are the quantum-mechanical results.

orbits yields very good agreement, except close to the boundary where the Friedel oscillations were not regularized.

In Fig. 9, we display selected contributions of some of the primitive orbits ($k=0$) to the particle density $\delta\rho(x,y)$. The solid line gives the contribution of self-retracing orbits with $\mathbf{p} = -\mathbf{p}'$ and the dashed line that of the other primitive NPOs. It is evident that no clear separation of regular short-ranged and irregular long-ranged oscillations can be made here.

IV. REGULARIZATION NEAR SURFACE

As we have pointed out in the previous section, the semiclassical approximation of density oscillations in terms of classical orbits breaks down near the classical turning point due to the diverging amplitude of the primitive + orbit (with
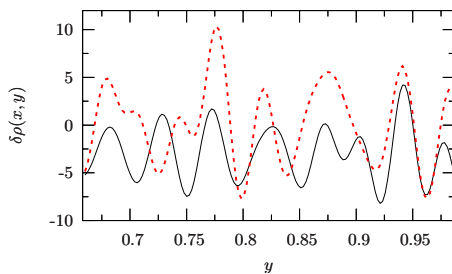

FIG. 9. (Color online) Same system as in Fig. 8. Here, selected contributions to Eq. (82) of the primitive NPOs with $k=0$ are shown. Full (black) line gives the contributions of the primitive self-retracing orbits and dashed (red) line that of all other primitive orbits.

$k=0$) which close to the surface is responsible for the Friedel oscillations. In order to regularize this diverging amplitude, different techniques must be used for smooth potentials and for billiards with reflecting walls.

A. Smooth potentials

In smooth potentials $V(\mathbf{r})$, the divergence can be regularized by linearizing the potential near the classical turning points, as it is done in the standard WKB approximation [39]. In the surface region close to a turning point, the exact results for linear potentials given in [28] can then be used. We demonstrate this first for the one-dimensional case and then illustrate it also for potentials in $D=3$ with spherical symmetry.

1. Linear approximation to a smooth 1D potential

We start from an arbitrary smooth binding potential $V(x)$ and approximate it linearly around the turning point x_λ defined by $V(x_\lambda) = \widetilde\lambda$. Without loss of generality, we assume $x_\lambda > 0$. Expanding $V(x)$ around x_λ up to first order in $x - x_\lambda$, we get the approximated potential

$$\widetilde V(x) = \widetilde\lambda + a(x - x_\lambda), \quad a = V'(x_\lambda) > 0. \tag{84}$$

We can therefore apply the results of [28]. The oscillating part of the density near the turning point then becomes

$$\delta\rho_{\mathrm{lin}}(x) = \rho_0\left\{[\mathrm{Ai}'(z_\lambda)]^2 - z_\lambda \mathrm{Ai}^2(z_\lambda) - \frac{1}{\pi}\sqrt{-z_\lambda}\,\Theta(x_\lambda - x)\right\}, \tag{85}$$

where the last term is the subtracted TF part and

$$\rho_0 = 2\left(\frac{2ma}{\hbar^2}\right)^{1/3}, \quad z_\lambda = \frac{\rho_0}{2}(x - x_\lambda). \tag{86}$$

The oscillating parts of the kinetic-energy densities $\tau(x)$ and $\xi(x)$ become in the same approximation

$$\delta\tau_{\mathrm{lin}}(x) = \frac{2a}{3}\left\{\mathrm{Ai}(z_\lambda)\mathrm{Ai}'(z_\lambda) - z_\lambda[\mathrm{Ai}'(z_\lambda)]^2 + z_\lambda^2 \mathrm{Ai}^2(z_\lambda) \right.$$
$$\left. - \frac{1}{\pi}|z_\lambda|^{3/2}\Theta(x_\lambda - x)\right\}, \tag{87}$$

$$\delta\xi_{\mathrm{lin}}(x) = -\frac{a}{3}\left\{\mathrm{Ai}(z_\lambda)\mathrm{Ai}'(z_\lambda) + 2z_\lambda[\mathrm{Ai}'(z_\lambda)]^2 - 2z_\lambda^2 \mathrm{Ai}^2(z_\lambda) \right.$$
$$\left. + \frac{2}{\pi}|z_\lambda|^{3/2}\Theta(x_\lambda - x)\right\}. \tag{88}$$

In the next step, we introduce uniform linearized approximations, in which the argument z_λ in Eqs. (85), (87), and (88) is not as given in Eq. (86) but replaced by

$$\widetilde z_\lambda = -[3S_+(x)/4\hbar]^{2/3}, \tag{89}$$

where $S_+(x)$ is the correct action of the + orbit for the given potential $V(x)$. One can show that this relation is exact for the linear potential; it is uniform for other smooth potentials
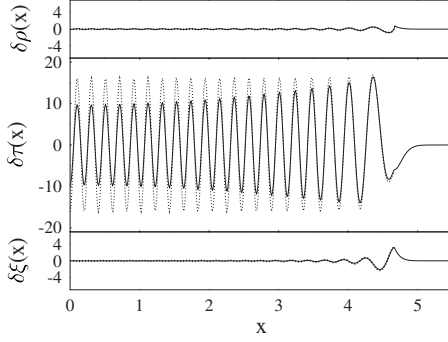
FIG. 10. Oscillating parts of densities for the quartic potential (53) with $N=40$ particles (units $\hbar=m=1$) shown on the same scale. (Solid lines) Exact quantum-mechanical results. (Dotted lines) Uniform linearized approximations (85), (87), and (88) with the argument $\tilde{z}_\lambda$ given in Eq. (89).
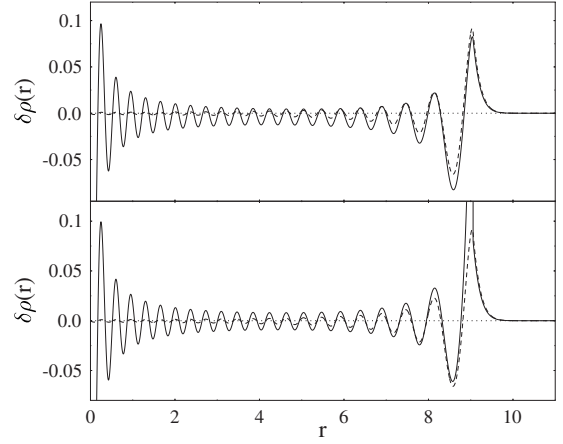

FIG. 11. Oscillating part of particle density for the 3D IHO with $N=22\,960$ particles ($M_s=40$) (units $\hbar=m=\omega=1$). (Solid lines) Exact results. (Dashed lines) Uniform linearized approximation (92) from [28] with argument $\tilde{z}_\lambda$ given in Eq. (93). (Upper panel) Smooth part in $\delta\rho(r)$ taken as TF density. (Lower panel) Smooth part in $\delta\rho(r)$ taken as ETF density.

in that it holds locally at the turning point and yields the correct phase of the oscillation at all other distances from the turning point.

Figure 10 shows numerical results for these uniform approximations for the quartic oscillator (53) with $N=40$ particles compared to the exact quantum results. We see that the uniform linearized approximation reproduces very well the Friedel oscillations near the turning point in all three densities. The phase of the oscillations is seen to be correct at all distances. The amplitudes are not exact in the asymptotic region, i.e., near $x=0$. This is not surprising since the contributions of all $-$ orbits and those of the $+$ with $k>0$ are missing in this approximation. We see that $\delta\xi(x)$ vanishes inside the system, as expected from the semiclassical leading-order result on the right-hand side of Eq. (51). However, near the turning point, where the semiclassical approximation breaks down, the magnitude of $\delta\xi(x)$ is comparable to—and for the quartic potential even larger than—that of $\delta\rho(x)$. (Note that all three density oscillations are shown on the same vertical scale.)

2. Linear approximation to smooth radially symmetric potentials in $D>1$

We now start from an arbitrary smooth binding potential with radial symmetry, $V(\mathbf{r})=V(r)$, $r=|\mathbf{r}|$, in $D>1$ dimensions. As above, we replace it by its linear approximation around the turning point r_λ analogously to Eq. (84)

$$\tilde{V}(\mathbf{r})=\tilde{\lambda}+\mathbf{a}\cdot(\mathbf{r}-\mathbf{r}_\lambda), \quad \mathbf{a}=\nabla V(r_\lambda). \quad (90)$$

Due to the spherical symmetry of $V(r)$, all components of the vector $\mathbf{a}$ have the same magnitudes

$$\mathbf{a}=a\mathbf{r}_\lambda/r_\lambda, \quad a=V'(r_\lambda). \quad (91)$$

Therefore, we may choose the radial variable r along any of the Cartesian axes x_i and the result

$$\rho(x_i)=-\frac{1}{48\pi}\rho_{i0}^3\{\text{Ai}(z_{i\lambda})\text{Ai}'(z_{i\lambda})+2z_{i\lambda}[\text{Ai}'(z_{i\lambda})]^2$$
$$-2z_{i\lambda}^2\text{Ai}^2(z_{i\lambda})\}, \quad (D=3) \quad (92)$$

where $\rho_{i0}=2\sigma_i a_i$, taken from [28] for the linear potential

with $D>1$, applies with the replacements $x_i\rightarrow r$, $z_{i\lambda}\rightarrow\sigma(ar-\lambda)$. As in Sec. IV A 1 for $D=1$, we may then subtract their ETF contribution. Finally, we introduce the uniform approximation to their oscillating parts near the surface with the argument (89) expressed in terms of the action $S_+(r)$ of the primitive radial $+$ orbit of the given radial potential $V(r)$,

$$\tilde{z}_\lambda=-[3S_+(r)/4\hbar]^{2/3}. \quad (93)$$

In Fig. 11, we show numerical results for this approximation for the three-dimensional (3D) IHO with $M_s=40$ occupied shells. The upper panel shows the exact result for $\delta\rho(r)$ (solid line), whereby only the TF approximation was used for its smooth part: $\delta\rho(r)=\rho(r)-\rho_{\text{TF}}(r)$. We notice that the oscillations in the interior are not symmetric about the zero line, which is due to smooth errors in the TF density. In the lower panel, the ETF corrections have been included in $\delta\rho(r)$; now the oscillations are symmetric about zero. The price paid for this is that $\delta\rho(r)$ diverges at the classical turning point. The uniform linear approximation (92) with the argument (93), shown in both panels by the dashed lines, reproduces well the Friedel oscillation near the surface. In the interior, it fails due to the missing contributions of the repetitions ($k>0$) of the $+$ and of all $-$ orbits. Once more, these results demonstrate that the Friedel oscillations near the surface are semiclassically explained by the primitive $+$ orbit alone. Its diverging amplitudes according to Eq. (40) must, however, be regularized by the uniform linear approximation.

In Fig. 12, we show the total density for the 3D IHO with $M_s=20$ filled shells. The solid line is the exact quantum result (2). The crosses give the semiclassical result as the sum $\rho_{\text{ETF}}(r)+\delta\rho(r)$, where the latter is calculated from the sum over the NPOs in Eq. (68) up to $k_{\text{max}}=15$. We see that the semiclassical result reproduces very accurately the exact result up to $r\sim5.9$, which is rather close to the turning point $r_\lambda\sim6.48$ where it diverges. The linearized approximation is
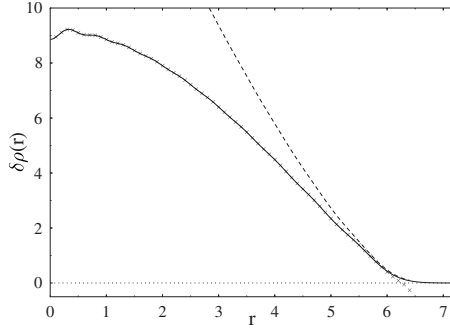
FIG. 12. Total particle density for the 3D IHO with $N=3080$ particles ($M_s=20$) (units $\hbar=m=\omega=1$). (Solid lines) Exact result. (Crosses) Semiclassical result for $\delta\rho(r)$ in Eq. (68), summed up to $k_{\max}=15$, plus $\rho_{\mathrm{ETF}}(r)$. (Dashed line) Uniform linearized approximation (92) from [28] with argument $\tilde{z}_\lambda$ in Eq. (93).

shown by the dashed line; it approximates the exact density closely above $r \sim 5.8$. Thus, switching from the semiclassical approximation to the linearized one around $r \sim 5.85$ allows one to obtain a very good approximation of the density in all points.

B. Billiard systems

In billiards with reflecting walls, the above linearization is not possible since the slope of the potential is always infinite at the classical turning points. The amplitude of the primitive + orbit can in such systems be regularized by using the following uniform approximation of the Green's function for short times [31,50]

$$G_{\mathrm{scl}}^{(\mathrm{un})}(E,\mathbf{r},\mathbf{r}') = \frac{m\pi}{i\hbar(2\pi\hbar)^{D/2}} \sum_\gamma \left| \frac{S}{p_\parallel p_\parallel'} \det\frac{\partial\mathbf{p}_\perp}{\partial\mathbf{r}_\perp'} \right|^{1/2} H_{D/2-1}^{(1)}(S/\hbar - \mu\pi/2), \tag{94}$$

where $H_\nu^{(1)}(x)$ is the Hankel function of the first kind. To evaluate the corresponding uniform approximation for the particle density, we have to take the imaginary part of Eq. (94) and perform the integration over the energy. This last step is not easily done analytically in general, since $H_\nu^{(1)}(x)$ is not a simple oscillatory function of the energy. In the following, we give results for the contributions to the particle density $\rho(\mathbf{r})$ in two special cases. Unfortunately, we have not been able to derive the corresponding contributions to the kinetic-energy densities.

1. Arbitrary 2D billiard

For billiards in $D=2$ dimensions with arbitrary boundaries, the uniform contribution to the particle density becomes (see [50] for details)

$$\delta\rho_+^{(\mathrm{un})}(d) = -\frac{p_\lambda J_1(2dp_\lambda/\hbar)}{2\pi\hbar d\sqrt{1-d/R}}, \tag{95}$$

where d is the distance from the boundary and R its curvature radius at the reflection point. Hereby, it is assumed that d is small enough so that there is only one + orbit going to the boundary and back to the given starting point. Note that

the curvature radius R is negative if the boundary is convex at the turning point.

2. Spherical billiards in D dimensions

For spherical billiards in D dimensions with radius R, the energy integral over Eq. (94) can also be performed and the regularized contribution of the primitive + orbit becomes

$$\delta\rho_+^{(\mathrm{un})}(r) = -\rho_{\mathrm{TF}}^{(D)} 2^\nu \Gamma(\nu+1) \left(\frac{R}{r}\right)^{\nu-1/2} \frac{J_\nu(z)}{z^\nu}, \tag{96}$$

where $\rho_{\mathrm{TF}}^{(D)}$ is the TF density given in Eq. (15) and

$$\nu = D/2, \quad z = 2(R-r)p_\lambda/\hbar. \tag{97}$$

For $D=3$, the expression (96) agrees with a result derived by Bonche [51] using the multiple-reflection expansion of the Green's function introduced by Balian and Bloch [52]. For $D=1$ (one-dimensional box), the result (96) is also found from the exact solution.

As mentioned above, the contribution (96) is responsible for the Friedel oscillations in the densities near the boundary $r=R$. It is interesting to perform the spatial integral of Eq. (96) over the volume of the billiard. Using the formula ([53], 6.561.14, with $\mu=-\nu$)

$$\int_0^\infty \frac{J_\nu(x)}{x^\nu} dx = \frac{1}{2^\nu} \frac{\Gamma(1/2)}{\Gamma(\nu+1/2)}, \tag{98}$$

the integral can be done in the limit $p_\lambda \to \infty$ (i.e., for large particle numbers) and the asymptotically leading term yields the following contribution to the particle number:

$$\delta N_{\mathcal{S}} \simeq -\frac{1}{2\pi^{D/2}\hbar^{D-1}} \frac{\Gamma(D/2)}{\Gamma(D)} p_\lambda^{D-1} \mathcal{S}_D, \tag{99}$$

where $\mathcal{S}_D$ is the hypersurface of the D-dimensional sphere

$$\mathcal{S}_D = \frac{2\pi^{D/2}}{\Gamma(D/2)} R^{D-1}. \tag{100}$$

We note that Eq. (99) corresponds precisely to the surface term in the Weyl expansion [54] of the particle number N. The Fermi energy λ_{TF} in Eq. (15) hereby has to be replaced by the corresponding quantity λ_{Weyl} obtained by integrating the Weyl-expanded density of states to the particle number N. The role of the + orbit in contributing the surface term to the Weyl expansion of the density of states has been demonstrated by Zheng [55] for arbitrary billiards in $D=2$ dimensions.

V. GENERAL RESULTS FOR FINITE FERMION SYSTEMS

After having presented our semiclassical theory for spatial density oscillations and tested it in various model potentials, we shall now discuss some of its results in the general context of finite fermion systems. Besides the trapped fermionic gases [1] mentioned already in Sec. I, we have in mind also self-bound molecular systems with local pseudopotentials, such as clusters of alkali metals [56], treated in the mean-field approach of DFT with the local-density approximation

(LDA), for which the KS potential is local [16].

A. Local virial theorem

One of our central results was given in Eq. (49) which we repeat for the present discussion

$$\delta\tau(\mathbf{r}) \simeq [\widetilde{\lambda} - V(\mathbf{r})]\delta\rho(\mathbf{r}). \tag{101}$$

We call it LVT because it connects the oscillating parts of the kinetic and potential-energy densities locally at any given point $\mathbf{r}$. While the well-known virial theorem relates, both classically and quantum mechanically, *integrated* (i.e., averaged) kinetic and potential energies to each other, the LVT in Eq. (101) does this *locally* at any point $\mathbf{r}$. We recall that hereby the Fermi energy $\widetilde{\lambda}$ of the averaged system is defined by Eq. (46).

Since no particular assumptions need be made [57] to derive Eq. (101) semiclassically from the basic Eqs. (40) and (41), the LVT holds for arbitrary local potentials and hence also for systems of interacting fermions in the mean-field approximation given by the DFT-LDA-KS approach. This is in itself an interesting basic result. It may also be of practical interest because it allows one to determine kinetic-energy densities from the knowledge of particle densities that in general are easier to measure experimentally. We leave it as a challenge to the condensed-matter community, in particular those working with trapped ultracold fermionic atoms, to verify the LVT experimentally.

Other forms of local virial theorems have been derived in [10] from the exact quantum-mechanical densities of isotropic harmonic oscillators in arbitrary dimensions. A Schrödinger-like (integro-) differential equation for the particle density $\rho(r)$ has also been derived in [10]. It would lead beyond the scope of the present paper to discuss these results and their generalization to arbitrary local potentials based upon our semiclassical theory. This will be done in a forthcoming publication [28], where we also give exact expressions for spatial densities in linear potentials of which we already have made use in Sec. IV.

B. Extended validity of the TF kinetic-energy functional

Presently, we discuss the direct functional relation (18) between the particle and kinetic-energy densities obtained in the Thomas-Fermi model. While Eq. (18) is exact only when applied to the TF expressions (15) and (17) of the (smooth) densities, we shall now show that a semiclassically approximate relation holds also between the oscillating exact densities

$$\tau(\mathbf{r}) \quad \simeq \quad \tau_{\text{TF}}[\rho(\mathbf{r})]. \tag{102}$$

Equation (102) states that the TF relation (18) holds approximately, for arbitrary local potentials $V(\mathbf{r})$, also for the *exact quantum-mechanical densities including their quantum oscillations*. This had been observed numerically already earlier [58], but without understanding of the reason for its validity.

The proof of Eq. (102) is actually very easy, having the LVT (101) at hand. Inserting $\rho(\mathbf{r}) = \rho_{\text{TF}}(\mathbf{r}) + \delta\rho(\mathbf{r})$ into Eq. (17) and Taylor expanding around $\rho_{\text{TF}}(\mathbf{r})$, we obtain
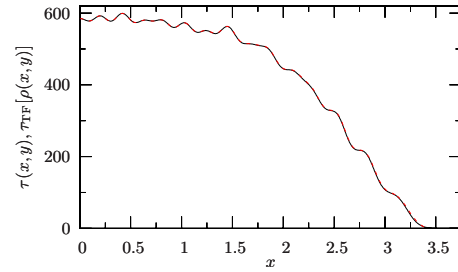

FIG. 13. (Color online) TF functional relation (102) for the same system as in Fig. 2 ($N=632$ particles). Cuts along the diagonal $x=y$. Solid (black) line is the left-hand side and dashed (red) line is the right-hand side of Eq. (102).

$$\tau_{\text{TF}}[\rho(\mathbf{r})] = \tau_{\text{TF}}[\rho_{\text{TF}}(\mathbf{r})] + \frac{d\tau_{\text{TF}}[\rho]}{d\rho}\bigg|_{\rho_{\text{TF}}(\mathbf{r})} \delta\rho(\mathbf{r}) + \mathcal{O}[(\delta\rho)^2]. \tag{103}$$

Using the obvious identity $\tau_{\text{TF}}[\rho_{\text{TF}}(\mathbf{r})] = \tau_{\text{TF}}(\mathbf{r})$ and the fact that $d\tau_{\text{TF}}[\rho_{\text{TF}}(\mathbf{r})]/d\rho_{\text{TF}}(\mathbf{r}) = [\widetilde{\lambda} - V(\mathbf{r})]$, we see immediately with Eq. (101) that, to first order in the oscillating parts, we have indeed the relation

$$\tau_{\text{TF}}[\rho(\mathbf{r})] \simeq \tau_{\text{TF}}(\mathbf{r}) + \delta\tau(\mathbf{r}) = \tau(\mathbf{r}). \tag{104}$$

We stress that, although the TF expression for all three kinetic-energy densities $\tau(\mathbf{r})$, $\tau_1(\mathbf{r})$, and $\xi(\mathbf{r})$ is the same [cf. Eq. (16)], the relation (102) holds only for $\tau(\mathbf{r})$. The reason is that the LVT also only holds for this kinetic-energy density, as discussed explicitly in the previous sections.

In Figs. 13 and 14, we present numerical tests of the relation (102) for the two-dimensional coupled quartic oscillator (50), which represents a classically chaotic system, with two different particle numbers. An example for the three-dimensional spherical billiard, which is a good approximation for the self-consistent mean field of very large alkali-metal clusters [18], is shown in Fig. 15. We see that in all cases, the relation (102) between the exact quantum-mechanical densities $\tau(\mathbf{r})$ and $\rho(\mathbf{r})$ is extremely well fulfilled; only close to the classical turning points, where the LVT (101) does not hold, do we see a slight deviation. Obviously, the terms of order $\mathcal{O}[(\delta\rho)^2]$, neglected in the above derivation, play practically no significant role in the interior of the systems—even for moderate particle numbers N as seen in Fig. 14 or in the examples given in Ref. [58] (and reproduced in [4]).
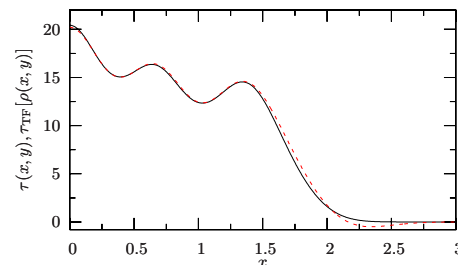

FIG. 14. (Color online) Same as in Fig. 13 for $N=42$ particles. Cuts along the line $y=x/\sqrt{3}$.
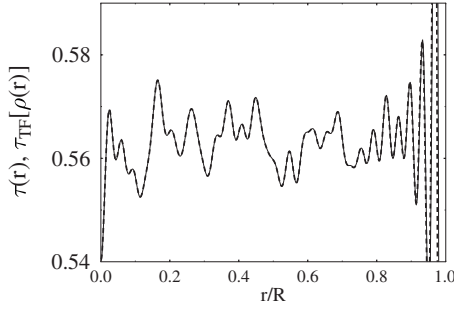
FIG. 15. Test of the TF functional relation (102) for $N = 100\,068$ particles in the three-dimensional spherical billiard (lines as in Fig. 14, units $\hbar^2/2m = R = 1$; both densities divided by $N^{5/3}$). Note that in the vertical direction of the figure, only a very small excerpt around the bulk value is displayed.

This result might come as a surprise, since it is well known from the ETF model that *for smooth densities,* the gradient corrections to the functional $\tau_{\rm TF}[\rho]$ do play an important role for obtaining the correct average kinetic energy. (For three-dimensional systems, the first of them is the famous Weizsäcker correction [59].) Examples for this are given in chapter 4.4 of [26]. However, if gradient corrections up to a given order were consistently added to Eq. (102) and used with the *exact* density $\rho(\mathbf{r})$, the agreement seen in the above figures would be completely spoiled.

VI. SUMMARY AND CONCLUDING REMARKS

We have presented a semiclassical theory, initiated in [19], for the oscillating parts of the spatial densities in terms of closed NPOs, while the smooth parts of the densities are given by the (extended) TF theory. Our Eqs. (40)–(42) are the analogs of the semiclassical trace formula (36) for the density of states in terms of periodic orbits.

For spherical systems, two kinds of oscillations in the spatial densities can be separated, as is implied in Eqs. (23)–(26): regular, short-ranged ones (denoted by the symbol $\delta_{\rm r}$) that we can attribute to the librating NPOs in the radial direction and irregular, long-ranged ones (denoted by $\delta_{\rm irr}$) that are due to nonradial NPOs and therefore only exist in $D > 1$ dimensions. The simple nature of the radial NPOs leads immediately to a number of relations between the regular parts of the oscillations, such as Eqs. (60) and (63) or the universal form (65) for $\delta_{\rm r}\rho(r)$ valid near $r = 0$. It also explains that the kinetic-energy density $\xi(r)$ defined in Eq. (6) has no rapid regular oscillations, as implied in Eq. (26), but is smooth for all one-dimensional systems, as well as for isotropic harmonic oscillators [10] and linear potentials [28] in arbitrary D dimensions, since these contain no nonradial NPOs.

In spherical systems, the semiclassical expansion in terms of NPOs is expected to work best for filled "main shells" where the total energy has a pronounced local minimum. This is also discussed in Ref. [21] on the two-dimensional circular billiard, for which a complete classification of all NPOs (in addition to the periodic orbits) has been made and the semiclassical theory for the spatial density oscillations

has been studied analytically. The semiclassical approximation for the density oscillations is, indeed, found there to work best for the closed-shell systems with filled main shells. But even for "midshells" systems with half-filled main shells and for most intermediate systems, the agreement of the semiclassical densities with the quantum-mechanical ones has turned out in [21] to be very satisfactory.

Based on the semiclassical theory, we were able to generalize the LVT given in Eqs. (49) and (101), which had earlier been derived from exact results for isotropic harmonic oscillators [10] to arbitrary local potentials $V(\mathbf{r})$. We emphasize that the LVT is valid (semiclassically) also for an *interacting N*-fermion system bound by the self-consistent Kohn-Sham potential obtained within the framework of DFT and might be verified experimentally in finite fermionic systems.

APPENDIX: INCLUSION OF FINITE TEMPERATURE IN THE SEMICLASSICAL THEORY

In this appendix, we give a short sketch of how to include finite temperatures in the semiclassical formalism. Extensions of semiclassical trace formulas to finite temperatures have been used already long ago in the context of nuclear physics [60] and more recently in mesoscopic physics [47]. We shall present here a derivation by means of a suitable folding function, which has proved useful also in the corresponding microscopic theory [61].

For a grand-canonical ensemble of fermions embedded in a heat bath with fixed temperature, the variational energy is the so-called grand potential Ω defined by [62]

$$\Omega = \langle \hat{H} \rangle - TS - \lambda \langle \hat{N} \rangle, \tag{A1}$$

where $\hat{H}$ and $\hat{N}$ are the Hamilton and particle number operators, respectively, T is the temperature in energy units (i.e., we put the Boltzmann constant k_B equal to unity), S is the entropy, and λ the chemical potential. Note that both energy and particle number are conserved only on the average. For noninteracting particles, we can write the Helmholtz free energy F as

$$F = \langle \hat{H} \rangle - TS = 2\sum_n E_n \nu_n - TS, \tag{A2}$$

where E_n is the energy spectrum of $\hat{H}$ and ν_n are the Fermi occupation numbers

$$\nu_n = \frac{1}{1 + \exp\left(\dfrac{E_n - \lambda}{T}\right)}, \tag{A3}$$

and the entropy is given by

$$S = -2\sum_n [\nu_n \log \nu_n + (1 - \nu_n)\log(1 - \nu_n)]. \quad (A4)$$

The chemical potential λ is determined by fixing the average particle number

$$N = \langle \hat{N} \rangle = 2\sum_n \nu_n. \quad (A5)$$

It can be shown [61] that the above quantities N, F, and S may be expressed in terms of a convoluted *finite-temperature level density* $g_T(E)$ as

$$F = 2\int_{-\infty}^{\lambda} E g_T(E) dE. \quad (A6)$$

The function $g_T(E)$ is defined by a convolution of the "cold" ($T=0$) density of states (13)

$$g_T(E) = \int_{-\infty}^{\infty} g(E') f_T(E - E') dE' = \sum_n f_T(E - E_n), \quad (A7)$$

whereby the folding function $f_T(E)$ is given as

$$f_T(E) = \frac{1}{4T \cosh^2(E/2T)}. \quad (A8)$$

Note that all sums in Eqs. (A2)–(A8) run over the complete (infinite) spectrum of the Hamiltonian $\hat{H}$. It is now easily seen that

$$N = 2\int_{-\infty}^{\lambda} g_T(E) dE. \quad (A9)$$

To show that the integral (A6) gives, indeed, the correct free energy (A2) including the "heat energy," $-TS$ needs some algebraic manipulations. From F, the entropy S can always be gained by the canonical relation

$$S = -\frac{\partial F}{\partial T}. \quad (A10)$$

The same convolution can now be applied also to the semiclassical trace formula (36) for the oscillating part of the density of states which we rewrite as

$$\delta g(E) \simeq \text{Re}\sum_{\text{PO}} \mathcal{A}_{\text{PO}}(E) \exp\left[\frac{i}{\hbar}S_{\text{PO}}(E) - i\sigma_{\text{PO}}\right]. \quad (A11)$$

The oscillating part $\delta g_T(E)$ of the finite-temperature level density is obtained by the convolution of Eq. (A11) with the function $f_T(E)$ as in Eq. (A7). In the spirit of the stationary-phase approximation, we take the slowly varying amplitude $\mathcal{A}_{\text{PO}}(E)$ outside of the integration and approximate the action in the phase by

$$S_{\text{PO}}(E') \simeq S_{\text{PO}}(E) + (E' - E)T_{\text{PO}}(E), \quad (A12)$$

so that the result becomes a modified trace formula

$$\delta g_T(E) \simeq \text{Re}\sum_{\text{PO}} \mathcal{A}_{\text{PO}}(E)\widetilde{f}_T[\mathcal{T}_{\text{PO}}(E)]\exp\left[\frac{i}{\hbar}S_{\text{PO}}(E) - i\sigma_{\text{PO}}\right], \quad (A13)$$

where

$$\mathcal{T}_{\text{PO}}(E) = T_{\text{PO}}(E)/\hbar \quad (A14)$$

and the temperature modulation factor $\widetilde{f}_T$ is given by the Fourier transform of the convolution function f_T,

$$\widetilde{f}_T(\mathcal{T}) = \int_{-\infty}^{\infty} f_T(\omega)e^{i\mathcal{T}\omega} d\omega. \quad (A15)$$

The Fourier transform of the function (A8) is known so that

$$\widetilde{f}_T(\mathcal{T}) = \frac{\pi T \mathcal{T}}{\sinh(\pi T \mathcal{T})}. \quad (A16)$$

The "hot" trace formula (A13) with the modulation factor (A16) has been obtained in [47,60].

For the spatial densities, we can proceed exactly in the same way. For the particle density, e.g., the microscopic expression (2) is replaced by

$$\rho_T(\mathbf{r}) = 2\sum_n |\phi_n(\mathbf{r})|^2 \nu_n, \quad (A17)$$

where the sum again runs over the complete spectrum. Starting from the semiclassical expression (40) for $\delta\rho(r)$ at $T=0$, we rewrite it as

$$\delta\rho_0(\widetilde{\lambda}, \mathbf{r}) \simeq \text{Re}\sum_{\text{NPO}} \mathcal{A}_{\text{NPO}}(\widetilde{\lambda}, \mathbf{r})\exp[i\Phi(\widetilde{\lambda}, \mathbf{r})], \quad (A18)$$

where the amplitude $\mathcal{A}_{\text{NPO}}$ collects all the prefactors of the phase in Eq. (40). The finite-T expression is given by the convolution integral

$$\delta\rho_T(\widetilde{\lambda}, \mathbf{r}) \simeq \int_{-\infty}^{\widetilde{\lambda}} \delta\rho_0(\widetilde{\lambda} - E, \mathbf{r}) f_T(E) dE. \quad (A19)$$

Expanding the phase under the integral as above, we arrive at

$$\delta\rho_T(\widetilde{\lambda}, \mathbf{r}) \simeq \text{Re}\sum_{\text{NPO}} \mathcal{A}_{\text{NPO}}(\widetilde{\lambda}, \mathbf{r})\widetilde{f}_T[\mathcal{T}_{\text{NPO}}(\widetilde{\lambda}, \mathbf{r})]\exp[i\Phi(\widetilde{\lambda}, \mathbf{r})], \quad (A20)$$

where $\mathcal{T}_{\text{NPO}} = T_{\text{NPO}}(\widetilde{\lambda}, \mathbf{r})/\hbar$ is the period of the NPO in units of $\hbar$. The corresponding expressions for the other spatial

densities are obvious.

For the smooth parts of the densities, we recall that the (E)TF theory at $T > 0$ is well known and refer to chapter 4.4.3 of [26] for the main results and relevant literature.

Other types of correlations can be included in the semiclassical theory in the same way, as soon as a suitable folding $f_{\text{corr}}(E)$ function corresponding to $f_T(E)$ in Eq. (A8) and its Fourier transform are known (see, e.g., Ref. [63]).

[1] B. DeMarco and D. S. Jin, Science **285**, 1703 (1999); B. De-Marco, S. B. Papp, and D. S. Jin, Phys. Rev. Lett. **86**, 5409 (2001); A. Görlitz *et al.*, *ibid.* **87**, 130402 (2001); A. G. Truscott *et al.*, Science **291**, 2570 (2001); F. Schreck, L. Khaykovich, K. L. Corwin, G. Ferrari, T. Bourdel, J. Cubizolles, and C. Salomon, Phys. Rev. Lett. **87**, 080403 (2001); C. A. Regal *et al.*, Nature (London) **424**, 47 (2003); M. W. Zwierlein, C. A. Stan, C. H. Schunck, S. M. F. Raupach, S. Gupta, Z. Hadzibabic, and W. Ketterle, Phys. Rev. Lett. **91**, 250401 (2003); C. A. Regal, M. Greiner, and D. S. Jin, *ibid.* **92**, 040403 (2004); M. W. Zwierlein *et al.*, Nature (London) **435**, 1047 (2005); G. B. Partridge *et al.*, Science **311**, 503 (2006).

[2] P. Vignolo, A. Minguzzi, and M. P. Tosi, Phys. Rev. Lett. **85**, 2850 (2000).

[3] F. Gleisberg, W. Wonneberger, U. Schlöder, and C. Zimmermann, Phys. Rev. A **62**, 063602 (2000).

[4] M. Brack and B. P. van Zyl, Phys. Rev. Lett. **86**, 1574 (2001).

[5] A. Minguzzi, N. H. March, and M. P. Tosi, Eur. Phys. J. D **15**, 315 (2001).

[6] A. Minguzzi, N. H. March, and M. P. Tosi, Phys. Lett. A **281**, 192 (2001).

[7] N. H. March and L. M. Nieto, Phys. Rev. A **63**, 044502 (2001).

[8] P. Vignolo and A. Minguzzi, J. Phys. B **34**, 4653 (2001).

[9] I. A. Howard, N. H. March, and L. M. Nieto, Phys. Rev. A **66**, 054501 (2002).

[10] M. Brack and M. V. N. Murthy, J. Phys. A **36**, 1111 (2003).

[11] E. J. Mueller, Phys. Rev. Lett. **93**, 190404 (2004).

[12] Z. Akdeniz, P. Vignolo, A. Minguzzi, and M. P. Tosi, Phys. Rev. A **66**, 055601 (2002).

[13] B. P. van Zyl, R. K. Bhaduri, A. Suzuki, and M. Brack, Phys. Rev. A **67**, 023609 (2003).

[14] P. Hohenberg and W. Kohn, Phys. Rev. **136**, B864 (1964).

[15] W. Kohn and L. J. Sham, Phys. Rev. **137**, A1697 (1965); **140**, A1133 (1965).

[16] M. R. Dreizler and E. K. U. Gross, *Density Functional Theory* (Springer-Verlag, Berlin, 1990).

[17] S. M. Reimann, M. Persson, P. E. Lindelof, and M. Brack, Z. Phys. B **101**, 377 (1996).

[18] M. Brack, Sci. Am. **277**, 50 (1997).

[19] J. Roccia and M. Brack, Phys. Rev. Lett. **100**, 200408 (2008).

[20] M. C. Gutzwiller, *Chaos in Classical and Quantum Mechanics* (Springer, New York, 1990).

[21] M. Brack and J. Roccia, J. Phys. A: Math. Theor. **42**, 355210 (2009).

[22] Note that in the standard literature on DFT, $\tau(\mathbf{r})$ sometimes denotes what we here call $\tau_1(\mathbf{r})$. See also Ref. [16], chapter 5.5, for a discussion and further literature on the various forms of the kinetic-energy density.

[23] R. K. Bhaduri and L. F. Zaifman, Can. J. Phys. **57**, 1990 (1979); C. Guet and M. Brack, Z. Phys. A **297**, 247 (1980).

[24] N. March, Adv. Phys. **6**, 1 (1957).

[25] J. G. Kirkwood, Phys. Rev. **44**, 31 (1933).

[26] M. Brack and R. K. Bhaduri, *Semiclassical Physics*, Revised ed. (Westview Press, Boulder, CO, 2003).

[27] In billiard systems with hard-wall reflection, there exists no gradient expansion of the potential and therefore the smooth parts of the densities are given by their TF values.

[28] M. Brack *et al.* (unpublished); cf. also Sec. VI in e-print arXiv:0903.2172.

[29] M. C. Gutzwiller, J. Math. Phys. **12**, 343 (1971).

[30] Conjugate points are those in which a fan of slightly perturbed orbits, obtained by small changes of the initial momentum (or position) of a given orbit, focuses again on the unperturbed orbit (see [20]).

[31] M. V. Berry and K. E. Mount, Rep. Prog. Phys. **35**, 315 (1972).

[32] S. C. Creagh and R. G. Littlejohn, Phys. Rev. A **44**, 836 (1991); A. Sugita, Ann. Phys. (N.Y.) **288**, 277 (2001); M. Pletyukhov and M. Brack, J. Phys. A **36**, 9449 (2003).

[33] S. C. Creagh, J. M. Robbins, and R. G. Littlejohn, Phys. Rev. A **42**, 1907 (1990).

[34] M. V. Berry and M. Tabor, Proc. R. Soc. London, Ser. A **349**, 101 (1976).

[35] M. Centelles, P. Leboeuf, A. G. Monastra, J. Roccia, P. Schuck, and X. Viñas, Phys. Rev. C **74**, 034332 (2006).

[36] M. V. Berry, Ann. Phys. (N.Y.) **131**, 163 (1981).

[37] W. Parry and M. Pollicott, Ann. Math. **118**, 573 (1983).

[38] B. Eckhardt and E. Aurell, Europhys. Lett. **9**, 509 (1989).

[39] A. B. Migdal, *Qualitative Methods in Quantum Theory* (W.A. Benjamin, Inc., Reading, 1977), Chap. 3.

[40] O. Bohigas, S. Tomsovic, and D. Ullmo, Phys. Rep. **223**, 43 (1993).

[41] A. B. Eriksson and P. Dahlqvist, Phys. Rev. E **47**, 1002 (1993).

[42] M. Gutiérrez, M. Brack, K. Richter, and A. Sugita, J. Phys. A **40**, 1525 (2007).

[43] V. M. Strutinsky and A. G. Magner, Sov. J. Part. Nucl. **7**, 138 (1976).

[44] For arbitrary radial potentials in $D > 1$, the determination of M_s is not as straightforward as for IHOs. It is, however, a well-known phenomenon that such systems exhibit nearly degenerate "main shells." See, e.g., M. Brack, J. Damgård, A. S. Jensen, H. C. Pauli, V. M. Strutinsky, and C. Y. Wong, Rev. Mod. Phys. **44**, 320 (1972). The values of M_s or the corresponding particle numbers N are best determined by looking for pronounced minima in the oscillating part $\delta E(N)$ of the total energy, the so-called "shell-correction energy."

[45] M. C. Gutzwiller, J. Math. Phys. **8**, 1979 (1967).

[46] P. Maslov and M. V. Fedoriuk, *Semiclassical Approximation in Quantum Mechanics* (Reidel, Dordrecht, 1981).

[47] K. Richter, D. Ullmo, and R. Jalabert, Phys. Rep. **276**, 1 (1996).

[48] The second derivatives of $\hat{S}$ with respect to $\mathbf{p}'_\perp$ together with Eq. (76) yield the expected determinant on the right-hand side of Eq. (32). Besides, the SPA also changes the topology of the classical trajectories in the phase space to have final position $\mathbf{r}'_\perp = \mathbf{r}_\perp$ instead of final momentum $\mathbf{p}'_\perp$. Note that the relation $\partial \hat{S}/\partial \mathbf{p}'_\perp = -\mathbf{r}'_\perp$ guarantees that the Legendre transformation (75) conserves Hamilton's equations of motion (i.e., that it corresponds to a canonical transformation).

[49] M. Abramowitz and I. A. Stegun, *Handbook of Mathematical Functions* (Dover, New York, 1970).

[50] O. Agam, Phys. Rev. B **54**, 2607 (1996).

[51] P. Bonche, Nucl. Phys. A. **191**, 609 (1972).

[52] R. Balian and C. Bloch, Ann. Phys. (N.Y.) **69**, 76 (1972).

[53] I. S. Gradshteyn and I. M. Ryzhik, *Table of Integrals, Series, and Products*, 5th ed. (Academic Press, New York, 1994).

[54] See, e.g., H. P. Baltes and E. R. Hilf, *Spectra of Finite Systems* (B.-I. Wissenschaftsverlag, Mannheim, 1976).

[55] W.-M. Zheng, Phys. Rev. E **60**, 2845 (1999).

[56] W. A. de Heer, W. D. Knight, M. Y. Chou, and M. L. Cohen, in *Solid State Physics* edited by H. Ehrenreich and D. Turnbull (Academic Press, New York, 1987), Vol. 40, p. 93; J. Pedersen, S. Bjørnholm, J. Borggreen, K. Hansen, T. P. Martin, and H. D. Rasmussen, Nature (London) **353**, 733 (1991); W. A. de Heer, Rev. Mod. Phys. **65**, 611 (1993); M. Brack, *ibid.* **65**, 677 (1993).

[57] We point out that the LVT holds also at critical points $\mathbf{r}$ connected with symmetry breaking and bifurcations, where the semiclassical amplitudes in Eqs. (40)–(42) have to be regularized by uniform approximations (cf. Sec. III E 3; see also Ref. [21] for the circular billiard).

[58] M. Brack in *From Nuclei to Bose Condensates* (University of Regensburg, Germany, 2000), p. 35.

[59] C. F. v. Weizsäcker, Z. Phys. **96**, 431 (1935).

[60] V. M. Kolomietz, A. G. Magner, and V. M. Strutinsky, Yad. Fiz. **29**, 1478 (1979); A. G. Magner, V. M. Kolomietz, and V. M. Strutinsky, Izv. Akad. Nauk SSSR, Ser. Fiz. **43**, 142 (1979).

[61] M. Brack and P. Quentin, Nucl. Phys. A. **361**, 35 (1981).

[62] Note that in this appendix, T and S without subscript denote temperature and entropy, respectively, while the same symbols with subscripts "PO" or "NPO" denote the periods and actions of the classical orbits as used everywhere else in this paper.

[63] M. Brack and J. Roccia, Int. J. Mod. Phys. E (to be published).